Extraction, Storage and Eruption of Multiple Isolated Magma Batches in the Paired Mamaku and Ohakuri Eruption, Taupo Volcanic Zone, New Zealand

F. BÉGUÉ[1]*, C. D. DEERING[2], D. M. GRAVLEY[1], B. M. KENNEDY[1], I. CHAMBEFORT[3], G. A. R. GUALDA[4] AND O. BACHMANN[5]

[1]DEPARTMENT OF GEOLOGICAL SCIENCES, UNIVERSITY OF CANTERBURY, PB 4800, CHRISTCHURCH 8140, NEW ZEALAND

[2]GEOLOGICAL AND MINING ENGINEERING AND SCIENCES, MICHIGAN TECH, 630 DOW ENVIRONMENTAL SCIENCES, 1400 TOWNSEND DRIVE, HOUGHTON, MI 49931, USA

[3]GNS SCIENCE, WAIRAKEI RESEARCH CENTRE, PB 2000, TAUPO 3352, NEW ZEALAND

[4]DEPARTMENT OF EARTH & ENVIRONMENTAL SCIENCES, VANDERBILT UNIVERSITY, NASHVILLE, TN 37240, USA

[5]INSTITUTE OF GEOCHEMISTRY AND PETROLOGY, DEPARTMENT OF EARTH SCIENCES, ETH ZURICH, CLAUSIUSSTRASSE 25, 8092 ZURICH, SWITZERLAND

The Taupo Volcanic Zone (TVZ) is well known for its extraordinary rate of rhyolitic magma generation and caldera-forming eruptions. Less is known about how large volumes of rhyolitic magma are extracted and stored prior to eruption, and the role tectonics might play in the process of melt extraction and control of caldera eruption(s). Here we present a new model for the extraction, storage and simultaneous eruption of the $>245\,km^3$ paired Mamaku and Ohakuri magmas sourced from calderas centred ~30 km apart (the Rotorua and Ohakuri calderas, respectively) in the central TVZ. The Mamaku and Ohakuri ignimbrites share a similar bulk pumice composition and the same phenocryst assemblage; however, bulk-rock compositions suggest several poorly mixed magma types in each erupted volume, which are randomly distributed throughout the eruptive deposits. To refine models of the pre-eruptive geometry of the magmatic system and discuss a possible origin for triggering of each eruption, we present an expanded database of matrix glass and quartz-hosted melt inclusion compositions along with the existing bulk-rock and mineral compositions. Major and trace element compositions show that the region produced five different magma batches, extracted from the same source region, and a continuous intermediate mush zone beneath the Mamaku–Ohakuri region is suggested here. These magma batches were most probably juxtaposed but isolated from each other in the upper crust, and evolved separately until eruption. The observed geochemical differences between the batches are likely to be generated by different extraction conditions of the rhyolitic melt from a slightly heterogeneous mush. The lack of evidence for more mafic recharge prior to eruption (for example, there are no bright cathodoluminescence rims on quartz crystals) suggests that a magmatic input is unlikely to be an eruption trigger. However, tectonic activity could be an efficient way to trigger the eruption of isolated magma batches, with the evacuation of one magma batch causing a disturbance to the local stress field and activating regionally linked faults, which then lead to the eruption of additional magma batches and associated caldera subsidence. In addition, the

*Corresponding author. Telephone: +64 21 02 22 1605. Fax: +64 3 364 2969. E-mail: florence.begue@pg.canterbury.ac.nz

extensional tectonic regime coupled with a high heat flux could be the controlling factor in the emplacement of some of the shallowest and most SiO$_2$-rich magmas on Earth.

INTRODUCTION

Caldera-forming eruptions commonly evacuate large volumes of silicic magma characterized by multiple pumice types with heterogeneous composition (e.g. Smith & Bailey, 1966; Lipman, 1967; Hildreth, 1981). How these different silicic magma types are generated, how they are stored, and what triggers their eruption are essential questions in understanding the magmatic processes associated with these large and potentially catastrophic events. The traditional model invoked to explain chemical heterogeneities within a large eruption is to have one large chemically layered magma chamber, which fractionates *in situ* (e.g. Bacon & Druitt, 1988; Hildreth, 1981; Brown *et al.*, 1998). However, an increasing number of studies suggest that an incrementally built reservoir, with the potential presence of discrete magma batches, may better explain these heterogeneities in certain systems, with *in situ* differentiation still playing an important role (e.g. Cambray *et al.*, 1995; Hildreth & Wilson, 2007; Lipman, 2007; Shane *et al.*, 2007; Miller *et al.*, 2011). These discrete batches may or may not interact prior to eruption, and may have unique magmatic histories (e.g. Reubi & Nicholls, 2005). In high-silica rhyolites, the differences between multiple magma batches can be challenging to detect because evidence based on mineral, glass and bulk chemistry is often subtle (e.g. Gualda & Ghiorso, 2013*b*). The 'mush model' for the petrogenesis of rhyolites involves interstitial melt extraction from upper crustal crystalline mush zones (e.g. Bachmann & Berganzt, 2004; Hildreth, 2004; Hildreth & Wilson, 2007), forming shallow cupolas of highly eruptible rhyolitic melt. Timescales related to crystal–melt segregation from a mush zone are important, and it is essential to distinguish between the time necessary to assemble and extract the rhyolitic melt from the mush (i.e. time to generate the melt and physically segregate it from the crystal mush), and the residence and crystallization time of that segregated melt until eruption. Finally, another important, and still poorly understood aspect in terms of hazard assessment is the trigger(s) of these very explosive eruptions. The critical overpressure for eruption may not be reached by volatile exsolution alone, and an input of more mafic magma into the chamber has been suggested by many researchers as another way to increase the internal pressure in the chamber, possibly leading to an eruption (e.g. Sparks *et al.*, 1977; Blake, 1981; Pallister *et al.*, 1992; Folch & Martí, 1998). A less frequently invoked model suggests a tectonic eruption trigger (e.g. Gravley *et al.*, 2007; Allan *et al.*, 2012); however, the relationship between regional tectonics and large ignimbrite eruptions is not well understood.

The central Taupo Volcanic Zone (TVZ) in New Zealand is a rifted arc in which rhyolitic volcanism has been linked to extensional tectonics (Wilson *et al.*, 2009). During an ignimbrite flare-up (∼340–240 ka; Gravley *et al.*, 2009, in preparation) seven distinct volcanic centres evacuated more than 3000 km^3 of high-silica rhyolite, and, although generally being fairly homogeneous (Dunbar & Kyle, 1989), small chemical heterogeneities have been identified in most of the resultant ignimbrites. The high-resolution chronostratigraphy and spatial distribution of ignimbrites in the TVZ present an ideal opportunity to study the origin of these heterogeneities and further decipher the relationship between magma emplacement, tectonics and volcanism. Paired eruptions are not uncommon in the central TVZ; the ∼60 ka Rotoiti and Earthquake Flat event is one well-documented example in which regional tectonics is implicated in back-to-back eruptions from two different vent sites, with a magma system composed of independent and unconnected magma bodies (Charlier *et al.*, 2003). Here we focus on another paired eruption sequence: the 240 ka Mamaku and Ohakuri eruptions that together evacuated more than 245 km^3 of rhyolitic magma (Milner *et al.*, 2003; Gravley *et al.*, 2007), and generated two separate caldera collapses 30 km apart. Both eruptive events produced heterogeneous bulk pumice compositions (involving three distinct magma types in each ignimbrite), but, remarkably, each of the recognized types can be found in both the Mamaku and Ohakuri ignimbrites (Milner *et al.*, 2003; Gravley *et al.*, 2007). We present a geochemical study of these ignimbrites to reconstruct their magmatic history and understand how the various magma types were assembled prior to their almost simultaneous eruption, and to identify potential eruption triggers. We show that not only did the Mamaku and Ohakuri eruptions evacuate multiple, chemically distinct, magma batches extracted from the same mush zone but also these batches evolved in isolation, despite being stored in reservoirs just a few kilometres apart.

GEOLOGICAL BACKGROUND

The TVZ is a rifted arc that reflects the subduction of the Pacific plate beneath the North Island of New Zealand, which is currently subject to NW–SE extension of 5–15 mm a^{-1} from SW to NE (Wallace *et al.*, 2004). The TVZ can be subdivided into three segments, with the northern and the southern segments dominated by andesitic volcanism typical of continental arcs. The 125 km × 60 km central segment is dominated by explosive caldera-forming rhyolitic volcanism, with only minor dacites and basalts erupted (Wilson *et al.*, 1995, 2009). More

than 6000 km^3 of rhyolite erupted over a period of ∼16 Myr (andesitic activity started ∼2 Myr ago; Houghton *et al.*, 1995; Wilson *et al.*, 1995). Rifting in the central TVZ started accelerating at ∼0·9 Ma (Wilson *et al.*, 1995), and is responsible for thinning of the crust and a heavily intruded lower crustal region from ∼16 to 30 km depth (i.e. Harrison & White, 2006). Rifting has also led to several extension-related graben structures segmented along the length of the central zone, in which a close relationship between tectonics, magmatism, and volcanism has been inferred from detailed field studies (Wilson *et al.*, 2009; Rowland *et al.*, 2010). The onset of accelerated rifting preceded or directly coincided with a transition to dominantly silicic volcanism (Wilson *et al.*, 1995; Deering *et al.*, 2011*a*), and caldera structures and their geometry are partially controlled by this regional extensional regime (Fig. 1a; e.g. the Okataina Volcanic Centre; Cole *et al.*, 2010; Seebeck *et al.*, 2010). Two types of rhyolite have been identified in the central TVZ, since the early work of Ewart (1965) and Ewart *et al.* (1975). Improved geochronology and more detailed bulk-rock and mineral chemistry have refined the chemical distinction, and a spatio-temporal distribution between 'wet-oxidizing' [rhyolite R1; crystal-rich (up to 45 vol. %); dominantly hydrous mineral phases (hornblende ± cummingtonite ± biotite); high fO$_2$ (ΔQFM = 1–2, where QFM is quartz–fayalite–magnetite)] and 'dry-reducing' [rhyolite R2; crystal-poor (<10 vol. %); dominantly anhydrous mineral phases (orthopyroxene ± clinopyroxene); low fO$_2$ (ΔQFM = 0–1)] rhyolite types has been proposed (Deering *et al.*, 2008, 2010). It has been suggested that the origin of these two end-member rhyolite types is related to subduction zone processes, with distinct slab-derived fluid fluxes in time and space (Deering *et al.*, 2010; Rooney & Deering, 2014).

An abrupt change in magmatism, volcanism and tectonics occurred at ∼340 ka, with an ignimbrite flare-up event that lasted until ∼240 ka (Gravley *et al.*, 2009, in preparation). During this flare-up more than 3000 km^3 of magma (almost half of the total erupted ignimbrite volume from the TVZ) erupted from at least seven calderas in the central TVZ (Gravley *et al.*, 2009). The Mamaku (>145 km^3; Milner *et al.*, 2003) and Ohakuri (>100 km^3; Gravley *et al.*, 2007) ignimbrites erupted during the last pulse of this flare-up, at ∼240 ka (Gravley *et al.*, 2007). They are sourced from the Rotorua and Ohakuri calderas, respectively, which are located on the western side of the central TVZ (Fig. 1). Interbedding of eruptive deposits, a lack of soil development and, most importantly, no trace of significant erosion between the Mamaku and Ohakuri deposits led Gravley *et al.* (2007) to suggest that the two eruptions occurred simultaneously. The eruption sequence began with the Ohakuri fall deposit (Unit 2 of Gravley *et al.*, 2007); its vent location, identified by isopleth maps for maximum pumice and lithic clast size, is near or within the Ohakuri caldera (Gravley *et al.*, 2007). This fall deposit is interbedded with the Mamaku ignimbrite, which erupted from the Rotorua caldera ∼30 km to the NE. No paleosol nor deep erosion is observed at the top of the Mamaku ignimbrite, suggesting a time break of only days to weeks before the emplacement of the Ohakuri ignimbrite. Field evidence provides a more accurate picture than the ^{40}Ar/^{39}Ar dates for both eruptions (240 ± 11 ka for the Mamaku ignimbrite and 244 ± 10 ka for the Ohakuri ignimbrite; Gravley *et al.*, 2007). Furthermore, a close relationship between caldera structures and rift tectonics has been identified. Paleogeomorphological reconstruction demonstrates that collateral subsidence occurred as part of the eruption sequence (Gravley *et al.*, 2007). The asymmetric geometry of the Rotorua caldera, which deepens considerably towards the SW (Milner *et al.*, 2002), and the prominent Horohoro fault scarp and associated depression (Fig. 1) provide morphological evidence of the relationship between volcanism and faulting between the Ohakuri and Rotorua calderas (Gravley *et al.*, 2007). The Horohoro fault runs through the Horohoro rhyolitic dome, situated on the inferred western margin of the Kapenga caldera (Fig. 1b). Field relationships show that the Mamaku ignimbrite was deposited around that dome, without over-topping it, demonstrating that the dome predates the Mamaku eruption (Milner, 2001). Part of the dome and the Mamaku ignimbrite have been displaced along the Horohoro fault, and field evidence supports syn-eruptive and/or immediately post-eruptive faulting, as the Ohakuri ignimbrite is thicker on the eastern side of the fault scarp (Gravley *et al.*, 2007). The subsidence of an ∼40 km^2 area adjacent to the Horohoro dome (Fig. 1b) is suggested to be related to lateral migration of magma towards the Ohakuri caldera (Gravley *et al.*, 2007). Lateral magma withdrawal may be a more common process in the rifting central TVZ than previously thought, as has recently been invoked for the Oruanui eruption from the Taupo Volcanic Centre (Allan *et al.*, 2012).

An important age constraint for magmatic processes related to the Ohakuri and Mamaku ignimbrites is the Pokai ignimbrite (∼275 ± 10 ka, ∼100 km^3; Wilson *et al.*, 2009). This ignimbrite, sourced from a composite structure known as the Kapenga caldera (Rogan, 1982; Wilson *et al.*, 1984; Karhunen, 1993), is separated from the Ohakuri and Mamaku deposits by a >30 cm thick, dark organic paleosol. The inferred boundary of the Kapenga caldera overlaps with the Ohakuri caldera to the south and incorporates the area of collateral subsidence between the Rotorua and Ohakuri calderas (Fig. 1), suggesting that the locations of the Pokai and the Mamaku–Ohakuri magmatic systems coincided. The time between these two events (∼275 to 240 ka) was also marked by a dome-building event (i.e. the Horohoro dome, located on
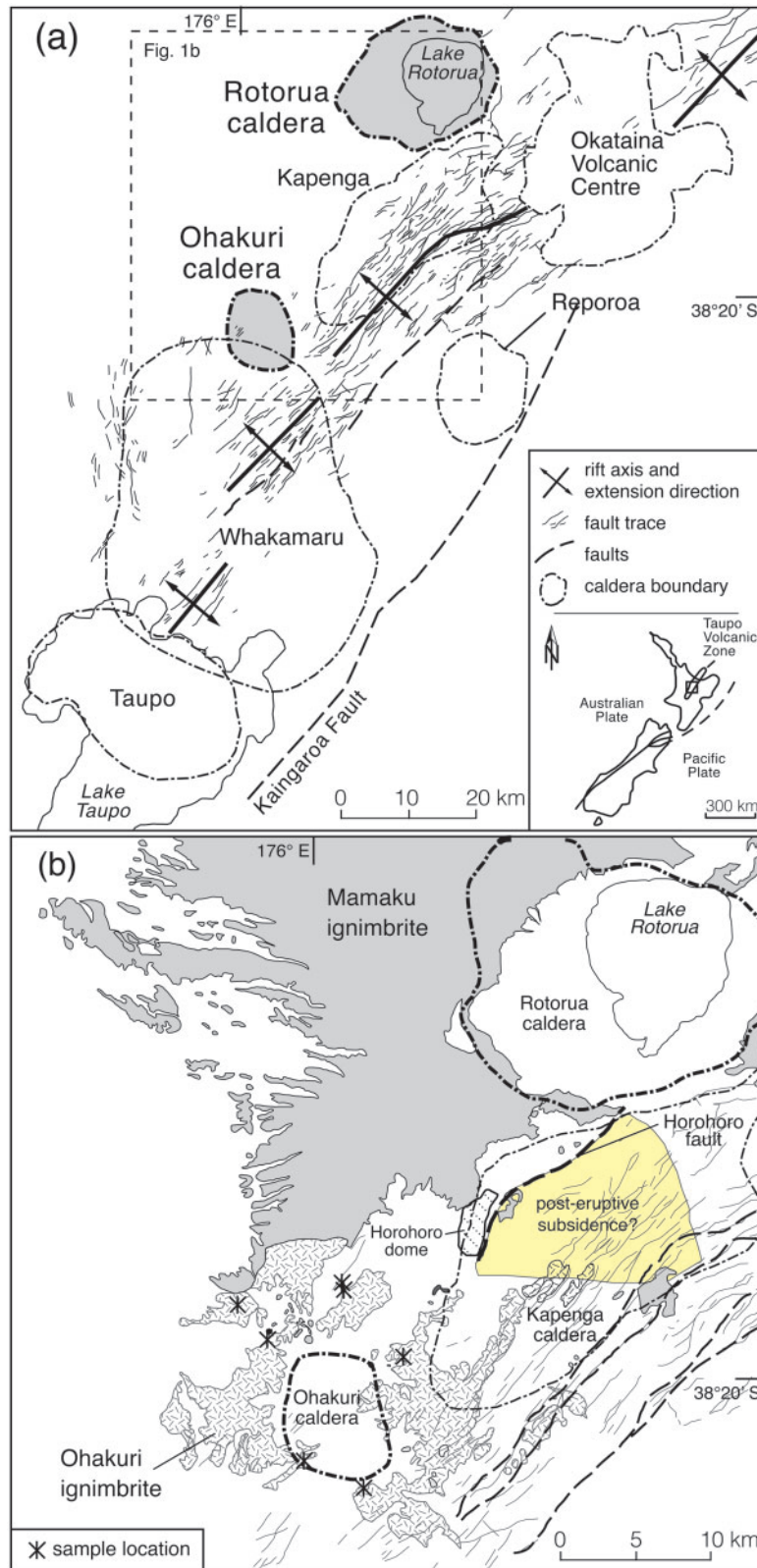
Fig. 1. (a) Map of the Taupo Volcanic Zone (TVZ), New Zealand. Caldera boundaries and structures after Rowland *et al.* (2010). (b) Geological map of the Ohakuri–Rotorua region and outline of the suggested post-eruptive subsidence area after Gravley *et al.* (2007); sample locations are marked with an asterisk.

the inferred western margin of the Kapenga caldera, Fig. 1b).

The Mamaku ignimbrite is physically very homogeneous (Milner, 2001; Milner *et al.*, 2003). The main sequence is predominantly massive, and it has been subdivided into three major units, with a non-welded, unconsolidated and pumiceous lower unit (lMI), through a largely welded middle unit (mMI), and to an intensely vapour-phase altered upper unit (uMI; Milner, 2001; Milner *et al.*, 2003). In contrast, Ohakuri is a non-welded, largely vitric ignimbrite, with complex stratigraphic depositional units showing dune bedding, mantling deposition, and evidence of energetic flows (Gravley, 2004; Gravley *et al.*, 2007). Three magma types have been identified in the Mamaku and Ohakuri deposits based on their bulk-rock compositions (Milner, 2001; Milner *et al.*, 2003; Gravley, 2004; Gravley *et al.*, 2007). These magma (pumice) types are found together at the same stratigraphic levels throughout the eruptive deposits and have the same lateral distribution, suggesting simultaneous eruption of all magma types (Milner *et al.*, 2003; Gravley, 2004). Strong chemical similarities between the Mamaku and Ohakuri rhyolites have been identified (Gravley, 2004; Gravley *et al.*, 2007), and will be further explored in this study.

ANALYTICAL METHODS
Sample preparation
We cleaned, oven-dried (50°C), and crushed 28 pumice clasts from the Ohakuri fall deposit and ignimbrite, and the Mamaku ignimbrite. As there is a lack of chemical stratification in both ignimbrites, no specific unit was targeted for pumice sampling (grid references of the sample locations are given in the Supplementary Data). To avoid the extensive vapour phase alteration (VPA) and devitrification that affects the middle and upper Mamaku ignimbrite (mMI and uMI; Milner *et al.*, 2003), only samples from the lower Mamaku ignimbrite were analysed. The various pumice types are very similar macro- and microscopically, and they can be identified only through chemical analysis. Therefore, samples were chosen based on the appearance of the pumice glass and degree of weathering; only fresh, pristine pumice clasts were selected for analysis.

Quartz crystals were handpicked and mounted in 1 inch (2·5 cm) epoxy mounts. To identify quartz-hosted melt inclusions we used immersion oil (refractive index 1·54) and chose only fully enclosed and glassy melt inclusions for analysis, which are larger than 50 μm to avoid boundary-layer effects (Roedder, 1984). Rare Mamaku and Ohakuri melt inclusions contained a vapour bubble; these inclusions were avoided for analyses.

Bulk-rock and mineral geochemistry
Bulk-rock and mineral chemistry data presented here represent a compilation from published work (Milner *et al.*,

2003; Deering *et al.*, 2008, 2010) and PhD theses (Milner, 2001; Gravley, 2004). Bulk-rock analyses were acquired for 175 samples by X-ray fluorescence spectrometry (XRF) at the University of Canterbury (157 samples; Gravley, 2001; Milner *et al.*, 2003) and Michigan State University (18 samples; Deering *et al.*, 2008). Inductively coupled plasma mass spectrometry (ICP-MS) was used to analyze Nb, Eu, Gd, Tb, Dy, Ho, Er, Yb, Lu, Hf, Ta, Y, Ba and Pb for 18 bulk-rock samples at Michigan State University (Deering *et al.*, 2008). Core and rim mineral composition was acquired by electron microprobe analysis (EPMA) at the University of Michigan (Cameca SX100; Deering *et al.*, 2008, 2010) and Victoria University of Wellington (Jeol Superprobe 733; Milner, 2001; Milner *et al.*, 2003).

Major element compositions of matrix glass and quartz-hosted melt inclusions
Major element compositions of glass shards from 28 pumice clasts and 157 quartz-hosted melt inclusions (in some cases multiple melt inclusions within the same quartz crystal) were acquired by electron microprobe (Jeol 733 Superprobe) at the University of Washington (UW). We used an acceleration voltage of 15 kV, a beam current of 5 nA, and a defocused beam of 10 μm diameter; we measured Na first in the analysis routine to minimize Na migration, although it can still occur at these conditions (Morgan & London, 1996). Counting times were 20 s for Si and P, and 40 s for the other major elements. The rhyolite glass VG 568 was used as a standard (Jarosewich *et al.*, 1980), and has been used to establish the standard error. Matrix glass analyses with totals lower than 95 wt % were discarded. For melt inclusions, average totals were ∼95 wt % (93–97·5 wt %). All reported results are normalized to 100% on an anhydrous basis. Analytical errors were <1% for SiO_2 and Al_2O_3, <3% for Na_2O and K_2O, and <7% for FeO and CaO. Titanium and manganese were below detection limit, which is 0·13 wt % for TiO_2, and 0·07 wt % for MnO.

Trace elements in quartz-hosted melt inclusions
We used the secondary ion mass spectrometer IMS Cameca 6f at Arizona State University (ASU) to analyse trace elements (Li, Rb, Sr, Y, Cs, Ba, La, Ce, Pr, Nd, Sm, Th and U) in 64 melt inclusions set in gold-coated epoxy mounts. The primary O^- beam intensity was set at 10 nA, and was focused to a spot of 10–20 μm diameter. The NIST 610 glass was used as a standard, being measured several times during each session. The composition of the standard was used to convert the measured trace element (relative to Si ratios) into concentrations (ppm). The analytical error was less than 3% for all elements, except for Th and U, for which the error was 10%.

Quartz cathodoluminescence

Quartz cathodoluminescence (CL) imaging was performed after the EMPA and secondary ion mass spectrometry (SIMS) analyses with a Gatan CL detector on a Jeol JSM-7000F scanning electron microscope at the University of Canterbury. The acceleration voltage was set at 15 kV, with a beam current ranging from 15 to 18 nA, and a working distance of 11 mm.

GEOCHEMICAL RESULTS

Bulk-rock geochemistry

Average major and trace element compositions of single pumice clasts are reported in Table 1. These data are combined with XRF bulk-rock composition from previously published work (Milner *et al.*, 2003) and unpublished theses (Milner, 2001; Gravley, 2004). The composition of pumice lapilli from the Ohakuri fall deposit could not be determined owing to the small size ($<$2 cm) of the samples.

We use the same terminology as previous researchers for the magma types of the Mamaku (Milner, 2001) and Ohakuri ignimbrites (Gravley, 2004); Type 3 represents the least evolved magma (65–72 wt % SiO_2), followed by Type 2 (70–75 wt % SiO_2), and finally the most evolved Type 1 (74–78 wt % SiO_2; Table 1). As reported by previous workers, the Type 1 and 2 magmas of the Ohakuri ignimbrite overlap in composition with the Type 1, 2 and 3 of the Mamaku ignimbrite; Ohakuri Type 3 is distinct and less evolved (Gravley *et al.*, 2007). The variations of Rb vs Sr in the bulk pumice are shown here to illustrate the three magma types (Fig. 2), which plot along different linear trend lines, and are separated by a compositional gap.

Mineral compositions

The Mamaku and Ohakuri rhyolites have the same phenocryst assemblage, which is predominantly plagioclase, quartz, orthopyroxene, and Fe–Ti oxides (Table 2). Representative compositions are summarized in Table 3.

Plagioclase

Plagioclase is the most abundant mineral phase in the Mamaku and Ohakuri deposits. It occurs as euhedral to subhedral tabular crystals, and forms single phenocrysts as well as glomerocrysts with orthopyroxene and Fe–Ti oxides. Mamaku plagioclase is normally zoned in all magma types (An_{31-17} for Type 1, An_{47-15} for Type 2, and An_{43-20} for Type 3; Milner *et al.*, 2003). Ohakuri plagioclase shows a very similar range, with An_{40-21} for Type 1, An_{38-22} for Type 2, and An_{46-20} for Type 3 (Fig. 3a). Ohakuri plagioclase overall appears to be slightly less potassic and encompasses a smaller CaO range (Fig. 3b). In general, the Mamaku and Ohakuri plagioclases have a lower An content than other documented TVZ plagioclase (Fig. 3a;

Schmitz & Smith, 2004; Deering *et al.*, 2008; Smith *et al.*, 2010).

Orthopyroxene

Orthopyroxene is found in every pumice type from the Mamaku and Ohakuri ignimbrites, and mostly has a stubby prismatic habit. It contains numerous mineral inclusions, which are frequently Fe–Ti oxides and apatite, but rare clinopyroxene inclusions also occur. The En contents [$Mg/(Mg + Ca + Fe)$] in the pyroxenes of the Mamaku and Ohakuri pumice clasts overlap from En_{40} to En_{54}, although the Mamaku samples have a second, smaller population of pyroxene with compositions of En_{58-64} (Fig. 4).

Glass geochemistry

Matrix glass

Matrix glass in the Mamaku (Ma) and Ohakuri (Oh) pumice clasts typically has a high-silica rhyolite composition, with SiO_2 contents ranging from 77 to 78·5 wt % for Mamaku Type 3, and from 78 to 80 wt % for Mamaku and Ohakuri Types 1 and 2, and the fall deposit (Fig. 5). Analyses with totals below 95 wt % were discarded, assuming secondary hydration and breakdown of the glass to clays. This criterion forced us to exclude all of the data for the Ohakuri Type 3 pumice. Average glass compositions and standard deviations are given in Table 4 (an extended dataset is available in the Supplementary Data; supplementary material is available for downloading at http://www.petrology.oxfordjournals.org).

The glass compositions of Types 3, 2 and 1 plot within three distinct CaO ranges, decreasing from Type 3 to 1 (Fig. 5). Type 2 pumices in the Mamaku and Ohakuri deposits are indistinguishable in terms of CaO. Likewise the Type 1 pumice CaO glass compositions in the Mamaku and Ohakuri deposits are similar and together plot close to the Ohakuri fall matrix glass. However, the SiO_2 contents of Type 1 and 2 glasses show a similar range (Figs 5 and 6). Na_2O and K_2O show similar groupings to CaO (Fig. 6), suggesting a trend towards more evolved compositions from Type 3 to Type 1. Within each pumice type, there is a strong decrease in Na_2O, and, to a smaller degree, in K_2O with increasing SiO_2 (Fig. 6).

Alkali loss (Fig. 6) may be the result of two distinct processes (apart from Na loss during analysis): (1) secondary hydration of the matrix glass, which will favour alkali migration (Cerling *et al.*, 1985); (2) plagioclase crystallization and fractionation. One way to test the influence of either process is to compare the melt inclusion composition with the matrix glass. For the Ohakuri eruptive deposits, we observe lower Na_2O and K_2O contents in the matrix glass (Fig. 6a–c); however, Al_2O_3 is higher in the matrix glass than in the melt inclusions (Fig. 6b). If plagioclase crystallization caused the alkali variability, Al_2O_3 would also be consumed by the reaction, and it should be lower in the

Table 1: Mamaku and Ohakuri average bulk pumice compositions

	Ohakuri						Mamaku					
	Type 1 XRF (n=46) ICP-MS (n=4)		Type 2 XRF (n=46) ICP-MS (n=4)		Type 3 XRF (n=8)		Type 1 XRF (n=17) ICP-MS (n=4)		Type 2 XRF (n=50) ICP-MS (n=6)		Type 3 XRF (n=8)	
	Av.	1σ	Av.	1σ	Av.	1σ	Av.	1σ	Av.	1σ	Av.	1σ
SiO_2	77·3	0·4	74·28	1·38	68·75	1·03	76·2	1·07	73·85	0·29	68·89	1·87
TiO_2	0·15	0·01	0·28	0·03	0·51	0·04	0·18	0·03	0·29	0·03	0·37	0·06
Al_2O_3	12·45	0·23	14·02	1·23	16·15	0·58	13·56	0·9	14·64	0·42	18·99	2·15
Fe_2O_3	1·46	0·05	2·32	0·27	3·6	0·39	1·57	0·23	2·29	0·21	3·07	0·38
MnO	0·05	0	0·07	0·01	0·12	0·02	0·06	0·01	0·07	0·02	0·09	0·02
MgO	0·2	0·05	0·35	0·06	0·72	0·06	0·15	0·08	0·3	0·06	0·38	0·17
CaO	0·73	0·03	1·39	0·16	2·8	0·26	0·83	0·17	1·24	0·22	1·7	0·31
Na_2O	3·67	0·23	3·81	0·44	4·75	0·33	3·79	0·12	4·06	0·13	4·09	0·35
K_2O	3·98	0·11	3·46	0·18	2·51	0·29	3·66	0·19	3·24	0·13	2·39	0·34
P_2O_5	0·01	0·01	0·03	0·01	0·08	0·04	0·01	0·01	0·02	0·01	0·02	0·01
LOI	4·4	1·13	3·55	0·48			4·97		3·16	0·28	4·17	1·42
Total	95·48	1·12	96·32	0·48			96·19	0·87	96·52	0·24		
Quartz (Q)	38·9	1·4	35·5	0·9	24·7	2·3	38·2	0·9	34·8	0·8	31·8	2·2
Orthoclase (Or)	23·5	0·6	20·4	1·1	14·9	1·7	21·6	1·1	19·1	0·8	14·1	2
Albite (Ab)	31	2	32·2	3·7	40·2	2·8	32	1	34·4	1·1	34·6	2·9
Anorthite (An)	3·6	0·1	6·7	0·8	13·4	1·5	4	0·8	6	1	8·3	1·6
Rb	125	7	108	9	85	17	111	8	94	3	70	30
Sr	58	2	121	13	244	26	72	18	114	14	133	62
Y	39	1	35	8	26	2	38	4	35	2	36	2
Ba	*837*	*69*	*822*	*23*	*634*	*17*	*792*	*74*	*761*	*53*	784	96
La	28	1	25	3	24	5	28	1	26	2	28	4
Ce	71	4	62	8	61	18	63	4	65	11	76	4
Pr	7	0	6	1			7	0	7	0		
Nd	26	1	24	4	38		26	0	25	2	29	8
Sm	6	0	5	1			6	0	5	0		
Th	14	0	12	1	17	5	14	1	13	2	13	2
U	4	0	3	0			4	0	3	0		
V	4	3	12	4	3	0	5	1	8	5	3	1
Cr	3	1	3	1	3	1	4	1	3	1	3	1
Ni	16	1	16	0			18		16	0		
Cu	3	2	7	4	72	4	1		27	17	76	35
Zn	40	2	47	5	14	2	71		56	4	17	3
Zr	167	9	250	7	181	48	190	28	279	27	218	69
Nb	*13*	*1*	*13*	*2*	9	1	*13*	*2*	*13*	*2*	11	2
Eu	*1*	*0*	*1*	*0*			*1*	*0*	*1*	*0*		
Gd	*6*	*0*	*5*	*1*			*6*	*0*	*6*	*0*		
Tb	*1*	*0*	*1*	*0*			*1*	*0*	*1*	*0*		
Dy	*5*	*0*	*5*	*1*			*6*	*0*	*5*	*0*		
Ho	*1*	*0*	*1*	*0*			*1*	*0*	*1*	*0*		
Er	*3*	*0*	*3*	*1*			*4*	*0*	*3*	*0*		
Yb	*4*	*0*	*3*	*1*			*4*	*0*	*4*	*0*		
Lu	*1*	*0*	*1*	*0*			*1*	*0*	*1*	*0*		
Hf	*5*	*0*	*6*	*0*			*5*	*1*	*6*	*1*		
Ta	*2*	*0*	*1*	*0*			*2*	*0*	*1*	*1*		
Pb	*39*	*3*	*29*	*3*	12	2	*42*	*8*	*37*	*7*	22	11

Major elements are given in wt % and trace elements in ppm. Compilation from published work (Milner *et al.*, 2003; Deering *et al.*, 2008, 2010) and PhD theses (Milner, 2001; Gravley, 2004); XRF was carried out at the University of Canterbury and Michigan State University; ICP-MS (at Michigan State University) was used for the analysis of Nb, Eu, Gd, Tb, Dy, Ho, Er, Yb, Lu, Hf, Ta, Y, Ba and Pb (in italics). LOI, loss on ignition.
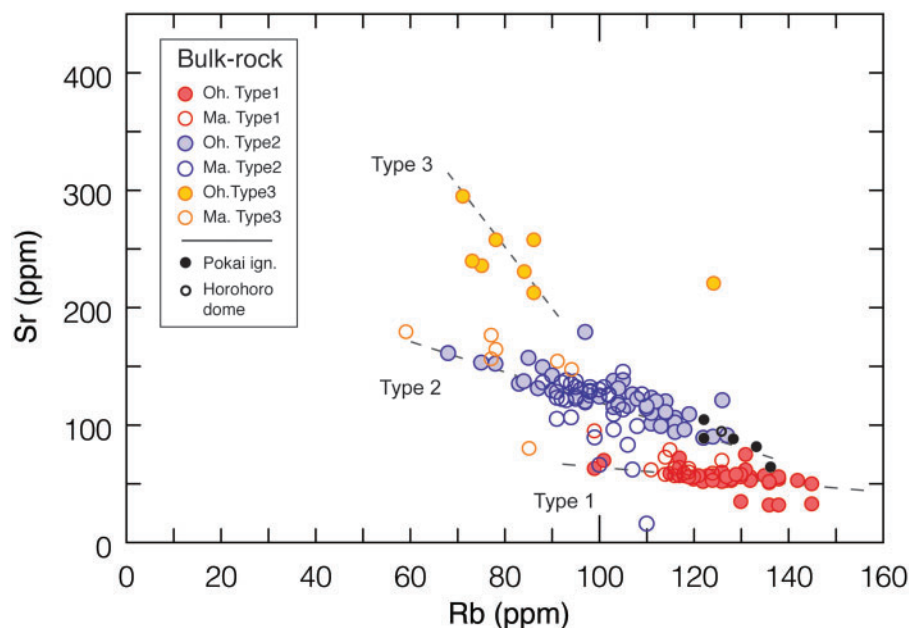
Fig. 2. Rb vs Sr from single-clast pumice bulk-rock analyses from the Mamaku (open symbols) and Ohakuri (filled symbols) deposits; data from Milner *et al.* (2003), Gravley (2004) and Deering *et al.* (2008).

Table 2: Mamaku and Ohakuri magma types

	Crystal content (vol. %)	Mineral assemblage	plg:qtz ratio
Ohakuri Type 1	<1*	plg + qtz + opx + Fe-Ti ox*	~1*
Ohakuri Type 2	<3-5*	plg + qtz + opx + Fe-Ti ox*	~2*
Ohakuri Type 3	10-15*	plg + qtz + opx + Fe-Ti ox ± *hbl**	~4*
Ohakuri fall deposit	–	plg + qtz + opx + Fe-Ti ox*	–
Mamaku Type 1	6-7*†	plg + qtz + opx + Fe-Ti ox ± *augite* ± *hbl*†	~2*
Mamaku Type 2	6-7*; 5-7†	plg + qtz + opx + Fe-Ti ox ± *augite*†	~2*
Mamaku Type 3	4-5†	plg + opx + Fe-Ti ox ± qtz ± *augite* ± *hbl*†	~8†

*Gravley (2004).
†Milner (2001).
plg, plagioclase; qtz, quartz; opx, orthopyroxene; ox, oxide. Italic type indicates minerals present in trace amount.

matrix glass compared with the melt inclusions. Secondary hydration seems to be a more plausible explanation, and the high SiO_2 and Al_2O_3 contents are thus an effect of the normalization, as they are the most abundant oxides. This is corroborated by the low analytical totals, especially for the Ohakuri matrix glass, which seems to be more affected than the Mamaku matrix glass. We also confirmed this by renormalizing the matrix glass composition using the same Na_2O and K_2O content as in the melt inclusions, which eliminated the effect of the higher Al_2O_3 content in the matrix glass compared with the melt inclusions. For this reason, in this study the matrix glass composition is used only for distinguishing between the magma types and to discuss magma mixing; it is not included in the establishment of the petrogenetic model.

Quartz-hosted melt inclusions

Average melt inclusion compositions are given in Tables 5 and 6 (an extended dataset is given in the Supplementary Data). Analysed melt inclusions are all high-silica rhyolite in composition, with SiO_2 contents ranging from 77·5 to 79·5 wt % (Figs 6 and 7). The melt inclusion analyses are subdivided into their respective magma types, according to the composition of the matrix glass in the host pumice

Table 3: Mamaku and Ohakuri representative mineral chemistry

	Eruption	Magma type	SiO$_2$	TiO$_2$	Al$_2$O$_3$	FeO	MnO	MgO	CaO	Na$_2$O	K$_2$O	Total	Ab%	An%	Or%	Mg#	En%	fO$_2$ (ΔNNO)	T (°C)
Plagioclase																			
D-90_plag1core	Ohakuri	Type 1	62·06		24·37	0·22			5·19	8·35	0·65	100·84	71·7	24·6	3·7				
D-90_plag1rim	Ohakuri	Type 1	62·18		25·00	0·23			5·28	8·33	0·61	101·63	71·5	25·0	3·4				
D-60_plag3core	Ohakuri	Type 2	61·15		24·37	0·23			5·39	8·34	0·48	99·95	71·7	25·6	2·7				
D-60_plag3rim	Ohakuri	Type 2	62·18		23·97	0·26			4·99	8·08	0·56	100·05	72·1	24·6	3·3				
D-87_plag2core	Ohakuri	Type 3	61·55		24·55	0·22			5·58	8·12	0·43	100·44	70·7	26·9	2·5				
D-87_plag2rim	Ohakuri	Type 3	61·88		24·02	0·23			4·95	8·35	0·61	100·04	72·7	23·8	3·5				
MKP35-1core	Mamaku	Type 1	62·55	–	23·17	0·33	0·06	–	4·96	8·51	0·50	100·16	73·5	23·7	2·8				
MKP35-1rim	Mamaku	Type 1	60·31	–	24·89	0·39	0·22	0·01	6·42	7·71	0·43	100·51	66·8	30·7	2·5				
MKP116-3core	Mamaku	Type 2	62·87	0·09	23·24	0·24	0·07	0·03	4·76	8·83	0·64	101·01	74·3	22·1	3·5				
MKP116-3rim	Mamaku	Type 2	63·31	0·10	22·99	0·34	0·04	0·04	4·21	8·85	0·63	100·51	76·4	20·1	3·6				
MPK29-1core	Mamaku	Type 3	63·65	0·06	24·67	0·31	0·04	0·03	5·79	5·66	0·40	100·69	62·0	35·1	2·9				
MPK29-1rim	Mamaku	Type 3	61·98	0·01	23·60	0·15	–	–	5·04	7·31	0·49	98·68	70·2	26·7	3·1				
Orthopyroxene																			
D-90_opx2core	Ohakuri	Type 1	49·96	0·08	0·16	34·43	2·37	12·95	0·98			100·92				40·1	39·3		
D-90_opx2rim	Ohakuri	Type 1	49·52	0·09	0·18	32·98	2·18	13·98	1·04			99·97				43·0	42·1		
D-60_opx2core	Ohakuri	Type 2	50·82	0·09	0·26	30·76	1·95	15·48	1·24			100·60				47·3	46·0		
D-60_opx2rim	Ohakuri	Type 2	51·08	0·17	0·53	28·77	1·56	16·72	1·30			100·14				50·9	49·5		
D-87_opx1core	Ohakuri	Type 3	52·48	0·18	0·74	23·45	1·25	21·56	1·12			100·77				62·1	60·7		
D-87_opx1rim	Ohakuri	Type 3	51·07	0·09	0·21	30·65	1·96	15·34	1·16			100·48				47·2	46·0		
MKP3-1core	Mamaku	Type 1	51·69	0·16	0·37	27·01	1·64	18·28	1·28			100·53				54·7	53·2		
MKP35-1rim	Mamaku	Type 1	50·46	0·12	0·26	30·48	2·47	15·50	1·17			100·53				47·6	46·4		
MKP116-1core	Mamaku	Type 2	49·72	0·21	0·33	31·80	2·07	14·79	1·14			100·10				45·3	44·2		
MKP116-1rim	Mamaku	Type 2	49·99	0·14	0·34	32·51	2·30	14·26	1·20			101·02				43·9	42·7		
MKP29-1core	Mamaku	Type 3	50·95	0·15	0·36	30·82	2·24	15·56	1·23			101·38				47·4	46·1		
MKP29-1rim	Mamaku	Type 3	51·30	0·10	0·27	31·01	2·27	15·04	1·23			101·40				46·4	45·1		

(continued)

Table 3: Continued

	Eruption	Magma type	SiO$_2$	TiO$_2$	Al$_2$O$_3$	FeO	MnO	MgO	CaO	Na$_2$O	K$_2$O	Total	Ab%	An%	Or%	Mg#	En%	fO$_2$ (ΔNNO)	T (°C)
Oxides																			
D-90__ox mt	Ohakuri	Type 1	0·11	10·97	0·97	80·51	0·70	0·43	0·02			93·72						-0·5	768
D-90__ox1ilm	Ohakuri	Type 1	0·04	47·61	–	47·28	1·47	1·05	0·00			97·45							
UC1204mt	Ohakuri	Type 2	0·10	11·65	1·09	81·43	0·78	0·54	0·00			95·70						-0·34	796
UC1204ilm	Ohakuri	Type 2	0·02	47·31	0·05	47·78	1·33	1·17	–			97·85							
D-87__ox1mt	Ohakuri	Type 3	0·06	11·04	1·17	80·86	0·76	0·58	0·03			94·50						0·21	799
D-87__ox2ilm	Ohakuri	Type 3	0·09	47·07	0·09	47·96	1·28	1·33	–			97·83							
UC1185mt	Mamaku	Type 1	0·06	11·37	1·11	79·98	0·77	0·56	0·02			94·25						-0·44	784
UC1185ilm	Mamaku	Type 1	0·01	47·55	0·06	47·41	1·30	1·24	0·01			97·78							
UC1176mt	Mamaku	Type 2	0·09	11·29	0·99	82·22	0·80	0·46	0·04			96·03						-0·27	793
UC1176ilm	Mamaku	Type 2	0·04	47·31	0·05	48·37	1·41	0·96	0·18			98·33							

Major elements are given in wt %. Data after Milner (2001), Gravley (2004) and Deering *et al.* (2008). Fe–Ti oxide geothermometry after Ghiorso & Evans (2008) for oxygen fugacity (*f*O$_2$) and temperature (*T*) calculations. Core and rim mineral chemistry was acquired by electron microprobe analysis (EPMA) at the University of Michigan (Cameca SX100; Deering *et al.*, 2008, 2010) and Victoria University of Wellington (Jeol Superprobe 733; Milner, 2001; Milner *et al.*, 2003).
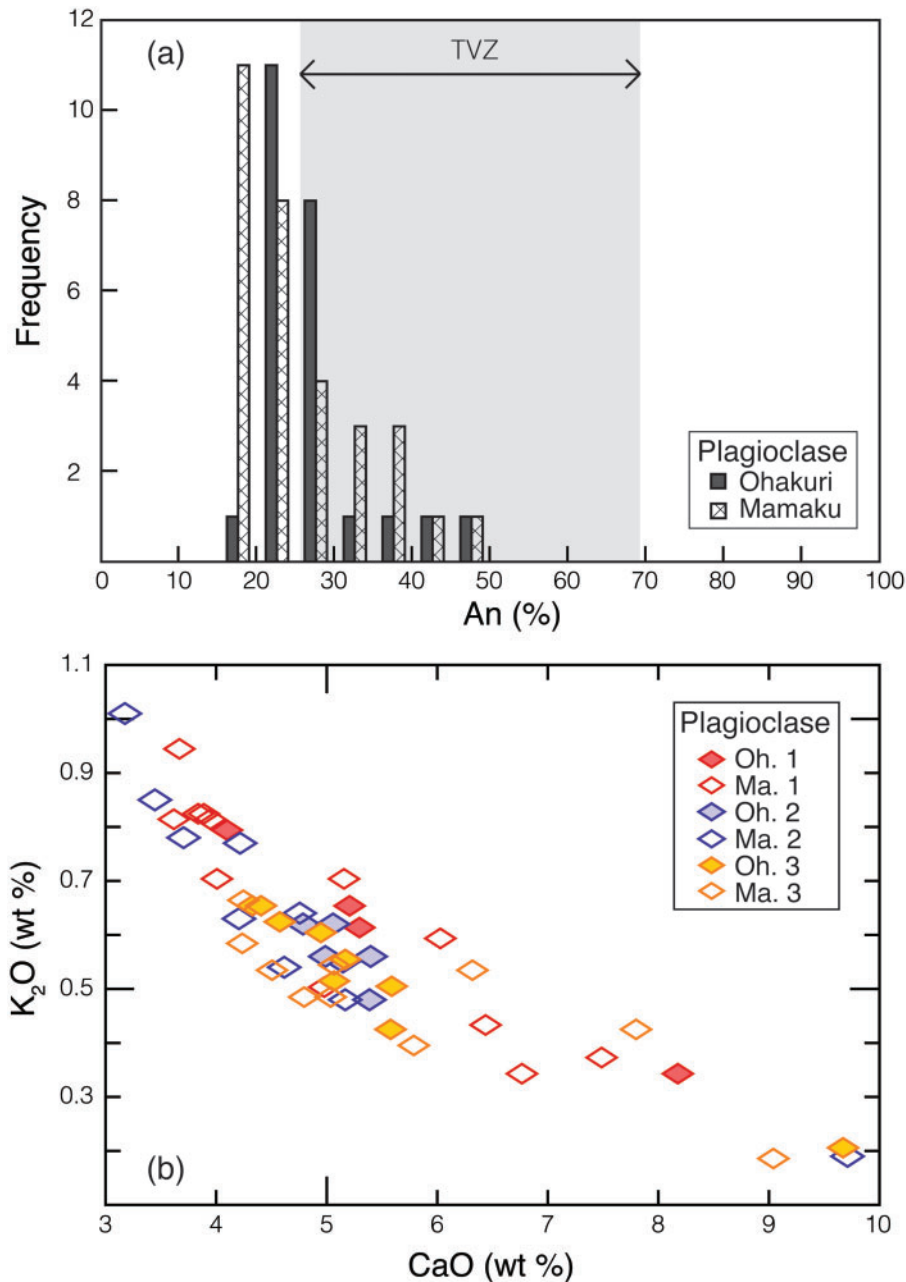
Fig. 3. Mamaku and Ohakuri plagioclase compositions. (a) An (%) vs frequency. Grey shaded band represents the An range for plagioclase in TVZ rhyolites (after Schmitz & Smith, 2004; Wilson *et al.*, 2006; Deering *et al.*, 2008; Smith *et al.*, 2010). (b) CaO vs K$_2$O for the Mamaku (open symbols) and Ohakuri (filled symbols) eruptions; data from Milner (2001) and Deering *et al.* (2008, 2010).

of each quartz grain. The Mamaku Type 3 melt inclusions examined in this study were all devitrified and, therefore, were not analysed. In contrast to the matrix glass, it is not possible to separate the magma types using the melt inclusion CaO content alone (Fig. 7a and c); however, Fig. 7a and c shows distinct negative trends within magma types. Each magma type has a small range (2 wt %) in silica content, and these ranges overlap between the types. The

Ohakuri fall deposit and most of the Mamaku Type 1 analyses plot at the lower SiO$_2$ end of the arrays. Furthermore, Type 1 melt inclusions in the Mamaku and Ohakuri have less SiO$_2$ than the Type 2 and the Ohakuri Type 3. The Ohakuri Type 3 has the least evolved bulk pumice chemistry, yet has melt inclusions with the highest SiO$_2$ content. In contrast to SiO$_2$, K$_2$O contents are higher in the Type 1 melt inclusions (Fig. 7b and d), and,
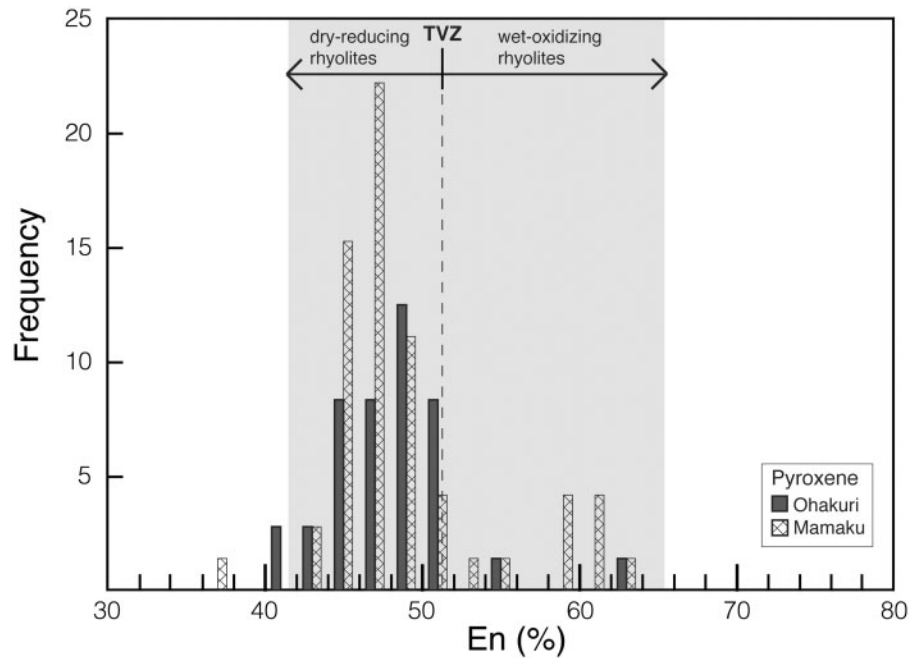
Fig. 4. Mamaku and Ohakuri pyroxene compositions; En (%) vs frequency. Grey field represents the En range for all central TVZ pyroxenes (after Deering *et al.*, 2008).
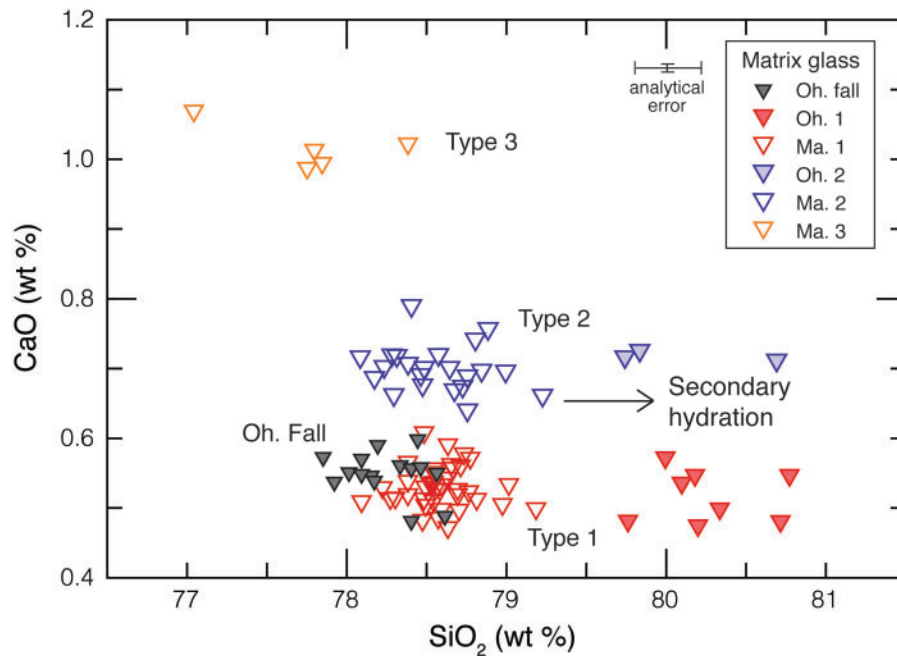
Fig. 5. Major element composition of the matrix glass in the Mamaku (open symbols) and Ohakuri (filled symbols) ignimbrites and fall deposit; data normalized on an anhydrous basis (analysis totals >95 wt %). Alkali loss owing to secondary hydration affects the normalization, thus accounting for the high SiO_2 content.

apart from a few outliers, Type 1 and Type 2 clearly plot into two different potassium fields. Ohakuri Type 3 plots within the potassium field of the Type 2 inclusions, and the Ohakuri fall inclusions plot with Type 1.

In Fig. 7b and d we observe a few outliers; melt inclusions from sample Ma2l (Mamaku pumice with a Type 1 matrix glass chemistry) plot with the Type 2 population (i.e. lower K_2O content; Fig. 7d); these four outliers

Table 4: Mamaku and Ohakuri average matrix glass compositions

	Ohakuri Fall deposit		Ohakuri Type 1		Ohakuri Type 2		Mamaku Type 1		Mamaku Type 2		Mamaku Type 3		SE* VG 568
	Av.	1σ	Av.	1σ	Av.	1σ	Av.	1σ	Av.	1σ	Av.	1σ	n = 35
SiO_2	78·24	0·23	80·25	0·34	80·08	0·52	78·58	0·21	78·56	0·29	77·76	0·48	0·148
TiO_2	0·08	0·05	0·09	0·05	0·16	0·05	0·07	0·05	0·11	0·06	0·17	0·08	0·011
Al_2O_3	12·16	0·12	12·17	0·10	12·04	0·05	12·03	0·11	12·04	0·16	13·15	0·19	0·137
FeO	1·07	0·05	1·09	0·07	1·24	0·07	1·03	0·05	1·23	0·06	1·39	0·10	0·117
MgO	0·06	0·01	0·06	0·01	0·10	0·00	0·06	0·01	0·08	0·01	0·13	0·03	0·006
CaO	0·55	0·03	0·52	0·04	0·72	0·01	0·53	0·03	0·70	0·03	1·02	0·03	0·002
Na_2O	3·66	0·14	2·11	0·24	2·15	0·41	3·54	0·13	3·61	0·10	3·21	0·39	0·006
K_2O	4·17	0·06	3·70	0·29	3·50	0·23	4·15	0·08	3·66	0·07	3·17	0·19	0·091
Total	95·47	0·33	95·40	0·32	96·34	0·67	95·96	0·51	95·80	0·47	96·44	1·26	0·026
Quartz (Q)	38·9		51·8		51·5		40·1	s	41·0		43·5		
Orthoclase (Or)	24·6		21·9		20·7		24·5		21·6		18·7		
Albite (Ab)	31·0		17·8		18·2		30·0		30·5		27·1		
Anorthite (An)	2·7		2·6		3·6		2·6		3·5		5·0		

Major elements are given in wt %. Analyses are normalized to anhydrous conditions. Total number of analysed pumice clasts was 28. Major element compositions determined by electron microprobe (Jeol 733 Superprobe) at the University of Washington (UW). Analytical conditions: acceleration voltage 15 kV, beam current 5 nA, and 10 μm beam diameter; counting times 20 s for Si and P; 40 s for all the other elements. Analytical errors: <1% for SiO_2 and Al_2O_3, <3% for Na_2O and K_2O, and <7% for FeO and CaO.
*Standard error = standard deviation divided by the square root of the number of samples.

represent analyses from three quartz crystals from the same pumice, whereas all other melt inclusions from that pumice plot with the Type 1 population. Equally, four data points for pumice Ma22 and one for pumice Ma25 (both have a Type 2 matrix glass composition) plot with the Type 1 population (i.e. high K_2O content in the melt inclusions; Fig. 7d). In Fig. 7b we observe two outliers of Type 2 pumice (sample Oh3 and Dl60) that have higher K_2O contents and plot with the Type 1 population; all other analysed melt inclusions from these two samples have K_2O concentrations consistent with Type 2. The water contents of the magmas can be estimated using the water by difference (WBD) method for the analysed melt inclusion compositions. Average WBD results (Table 5) range between 3·8 and 5·6 wt %, with errors of ±1 wt %.

The most notable variations in melt inclusion composition between the magma types from the Mamaku and the Ohakuri lie in the trace elements. The Rb/Sr ratio is in the range of 3–8, and it is positively correlated with SiO_2 content for each pumice type (Fig. 8a). The trends are steep and distinct, but subparallel for Type 1 Mamaku, Ohakuri, and the Ohakuri fall deposit. In contrast, Type 2 magmas have a low Rb/Sr ratio and a shallow slope (except for a few outliers). Type 3 Ohakuri has the same

range in Rb/Sr ratio as Type 1 pumice. The observed outliers (predominantly Mamaku samples), displaying high Rb/Sr and high SiO_2, each represent a melt inclusion from a different pumice clast.

Mamaku and Ohakuri can be distinguished based on distinct U contents in the melt inclusions, with values below 1 ppm for all Mamaku types, and values between 2 and 3·5 ppm for all Ohakuri types, including the fall deposit (Fig. 8b). Cs contents are higher in the Mamaku melt inclusions (4–7 ppm) than in Ohakuri types 1, 2 and 3 (2·5–5·5 ppm; Fig. 8b and c). Cs contents in the Ohakuri fall deposit (5–6 ppm) overlap with the Mamaku inclusions. Li behaves similarly to Cs, with a higher content in the Mamaku melt inclusions and Ohakuri fall deposit (Li values from 60 to 90 ppm), and values that plot below 60 ppm for the Ohakuri melt inclusions (Fig. 8c).

Bulk-pumice and melt inclusion compositions are compared in Fig. 9. The Mamaku and Ohakuri Type 1 bulk-pumice compositions are very similar to those of the melt inclusions, with some overlapping data points (Fig. 9a and b), which is consistent with the low crystallinity of Type 1 (Table 2). In contrast, the bulk pumice and melt inclusion compositions for Ohakuri Type 2 and 3 and for Mamaku Type 2 plot as distinct clusters (Fig. 9c and d). Melt inclusion compositions are more evolved than the
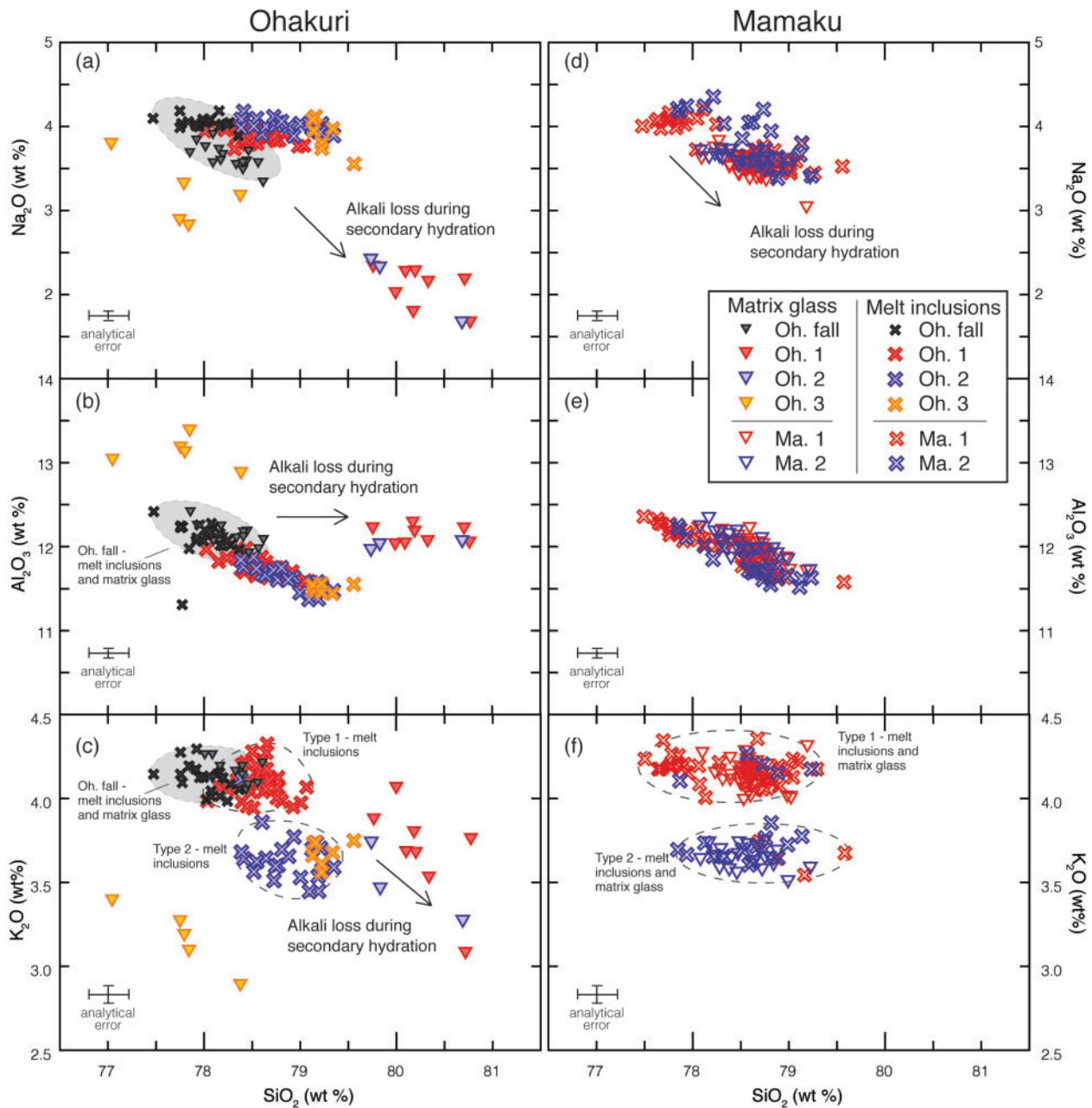
Fig. 6. Major element compositions of the matrix glass and the melt inclusions. (a–c) Ohakuri eruptive deposits (filled symbols); (d–f) Mamaku ignimbrite (open symbols); all data normalized on an anhydrous basis. The matrix glass compositions of the Ohakuri eruptive deposits are affected by alkali loss during secondary hydration, as shown in (a)–(c). This also affects the normalizations, resulting in high SiO_2 and Al_2O_3 contents in (b). Melt inclusion outliers with more than 80 wt % SiO_2 were not plotted.

bulk pumice, which is shown by the selected elements in Fig. 9, with lower MgO and Sr in the melt inclusions.

Cathodoluminescence (CL)

CL images were obtained for 92 quartz grains (48 from the Ohakuri pumice, including the fall deposit, and 44 from the Mamaku pumice); almost all imaged quartz is

surrounded by glass, indicating that the observed crystal habits are primary. These CL images are essential to understanding quartz growth history and changes in conditions experienced by the quartz crystals. The intensities of the CL zones are related to chemical impurities in the quartz lattice (e.g. Peppard *et al.*, 2001; Landtwing & Pettke, 2005). For volcanic quartz, some CL zones have

Table 5: Average major element composition for Mamaku and Ohakuri quartz-hosted melt inclusions

	Ohakuri Fall deposit $n = 19$ from 5 clasts, 16 quartz crystals		Ohakuri Type 1 $n = 35$ from 4 clasts, 25 quartz crystals		Ohakuri Type 2 $n = 22$ from 4 clasts, 20 quartz crystals		Ohakuri Type 3 $n = 8$ from 1 clast, 4 quartz crystals		Mamaku Type 1 $n = 43$ from 6 clasts, 30 quartz crystals		Mamaku Type 2 $n = 21$ from 3 clasts, 13 quartz crystals		SE* VG 568 $n = 35$
	Av.	1σ	Av.	1σ	Av.	1σ	Av.	1σ	Av.	1σ	Av.	1σ	
SiO_2	78·00	0·21	78·55	0·22	78·85	0·30	79·47	0·59	78·54	0·69	78·59	0·40	*0·148*
TiO_2	0·08	0·04	0·10	0·05	0·12	0·05	0·14	0·06	0·13	0·08	0·13	0·06	*0·011*
Al_2O_3	12·14	0·12	11·77	0·10	11·63	0·14	11·37	0·36	11·86	0·33	11·80	0·21	*0·137*
FeO	0·94	0·07	1·01	0·09	1·09	0·11	0·96	0·09	0·98	0·08	1·06	0·07	*0·117*
MnO	0·05	0·02	0·04	0·02	0·04	0·03	0·03	0·01	0·04	0·03	0·06	0·02	*0·006*
MgO	0·06	0·01	0·06	0·01	0·07	0·02	0·05	0·02	0·05	0·02	0·06	0·02	*0·002*
CaO	0·55	0·05	0·54	0·06	0·61	0·05	0·54	0·05	0·53	0·07	0·61	0·08	*0·006*
Na_2O	4·05	0·07	3·88	0·07	4·01	0·07	3·87	0·18	3·73	0·30	3·87	0·29	*0·091*
K_2O	4·12	0·08	4·10	0·10	3·65	0·14	3·61	0·18	4·13	0·17	3·82	0·21	*0·026*
Total	94·11	0·37	95·26	0·35	95·52	0·64	95·98	0·48	94·56	0·82	94·80	0·60	
WBD	5·65	0·40	4·55	0·39	4·21	0·72	3·81	0·44	5·31	0·80	5·02	0·66	
Quartz (Q)	36·7	0·7	38·3	0·6	39·4	0·9	41·2	1·9	39·1	2·6	39·2	1·8	
Orthoclase (Or)	24·3	0·5	24·2	0·6	21·6	0·8	21·3	1·1	24·4	1·0	22·6	1·3	
Albite (Ab)	34·3	0·6	32·8	0·6	33·9	0·6	32·7	1·5	31·6	2·6	32·8	2·5	
Anorthite (An)	2·6	0·3	2·5	0·3	2·8	0·2	2·5	0·4	2·5	0·4	2·9	0·5	

Major elements are given in wt %; analyses are normalized to anhydrous conditions. Major element compositions determined by electron microprobe (Jeol 733 Superprobe) at the University of Washington (UW). Analytical conditions: acceleration voltage 15 kV, beam current 5 nA, and 10 μm beam diameter; counting times 20 s for Si and P; 40 s for all the other elements. WBD, water by difference. Analytical errors: <1% for SiO_2 and Al_2O_3, <3% for Na_2O and K_2O, and <7% for FeO and CaO. Ti and Mn were below detection limit (0·13 wt % for TiO_2, and 0·07 wt % for MnO).
*Standard error = standard deviation divided by the square root of the number of samples.

been shown to correlate well with the Ti concentration, which in turn reflects the formation temperature and Ti activity of the melt (Wark & Watson, 2006), pressure (Thomas *et al.*, 2010), and growth rate (Huang & Audétat, 2012), and therefore can provide valuable information on magma chamber processes (e.g. Matthews *et al.*, 2011; Wilcock *et al.*, 2012).

The imaged quartz crystals are euhedral to subhedral, with slight embayments on some of the pyramidal faces (Fig. 10a and e–n). Large variation in CL patterns is observed between quartz crystals. A core zone is present in more than 95% of the imaged quartz and we can distinguish three core types: (1) rounded cores (~40 grains), overall slightly brighter, often displaying oscillatory zoning (Fig. 10g, m and o–r) that is truncated by the next CL zone; (2) jagged cores (~20 grains) with very irregular boundaries (Fig. 10f, i and l), often displaying oscillatory zoning, some cores are very bright (~10 grains; Fig. 10q and s); (3) skeletal cores (~15 grains) with generally darker CL intensities (Fig. 10e and k). A dark CL zone

almost always surrounds these cores, filling the irregularities and forming an outline that parallels the crystal face (Fig. 10f, h, j, o–p and r).

The jagged boundaries of the core and the discordant zoning with the surrounding zones suggest a partial melting event. Oscillatory concentric zoning is ubiquitous throughout the quartz crystals (e.g. Fig. 10q), with an alternation between bright and dark CL zones, parallel to each other. Bright rims (50–150 μm) can be observed on a few of the crystals (7 grains; Fig. 10h, j, n and t). These rims are either concordant with the previous zone (Fig. 10j), or surround rounded core zones (Fig. 10j and n). Late-stage skeletal growth, which is presumably related to rapid growth, is present on 6 grains (Fig. 10m and t). The bright rims and late-stage skeletal growth patterns have not been observed in the imaged quartz from the Ohakuri Type 1 and fall deposit. Rare crystals (three grains) have a thin bright rim (<10 μm), which is only partially present on one face of the crystal (Fig. 10s). However, it is important to note here that the presence of the bright rims is not

Table 6: Average trace element composition for Mamaku and Ohakuri quartz-hosted melt inclusions

	Ohakuri Fall deposit $n=11$ from 5 clasts, 9 quartz crystals		Ohakuri Type 1 $n=14$ from 4 clasts, 12 quartz crystals		Ohakuri Type 2 $n=13$ from 4 clasts, 12 quartz crystals		Ohakuri Type 3 $n=4$ from 1 clast, 2 quartz crystals		Mamaku Type 1 $n=12$ from 6 clasts, 9 quartz crystals		Mamaku Type 2 $n=6$ from 3 clasts, 5 quartz crystals		SE* NIST 610 $n=13$
	Av.	1σ	Av.	1σ	Av.	1σ	Av.	1σ	Av.	1σ	Av.	1σ	
Li	63	8	53	3	37	9	41	4	75	8	73	2	*3*
Rb	123	5	122	11	106	8	132	10	122	7	115	10	*7*
Sr	24	4	25	5	31	4	24	3	25	6	29	8	*6*
Y	30	1	30	1	28	2	30	1	30	1	29	0	*4*
Cs	6	0	4	1	4	0	4	1	5	1	5	0	*6*
Ba	619	10	610	30	576	24	616	29	624	23	577	12	*6*
La	23	1	23	1	22	2	23	1	23	1	22	1	*7*
Ce	48	2	49	2	45	3	49	2	49	2	46	1	*3*
Pr	5	0	5	0	5	0	5	1	6	0	5	0	*5*
Nd	19	1	19	1	17	2	19	1	20	1	18	0	*5*
Sm	4	1	4	1	4	1	4	0	5	0	4	0	*29*
Th	11	1	11	1	10	1	10	1	11	1	10	1	*11*
U	2	1	3	0	2	1	3	0	1	0	1	0	*11*

Trace elements are given in ppm. SIMS analyses with an IMS Cameca 6f (Arizona State University); 10 nA beam intensity, 10-20 μm spot size. Analytical error: <3% for all elements, and ~10% for Th and U.
*Standard error = standard deviation divided by the square root of the number of samples.

pervasive throughout the same pumice clast (i.e. quartz crystals that are presumably located close to each other in the magma chamber just prior to eruption do not all record the same event in their outermost zones). Mamaku samples generally have more complex zoning than the Ohakuri samples, with sometimes more than one partially resorbed horizon (8 grains; Fig. 10l and t). The frequency of these CL zoning patterns for each pumice type is summarized in Fig. 11.

Melt inclusions are nearly always found in the dark CL zones surrounding the core zone, which has also been observed in the quartz crystals from the Oruanui eruption (Taupo Volcanic Centre, Liu *et al.*, 2006). Those present in the vicinity of the crystal rims are mostly re-entrants (Fig. 10a–c and m). Melt inclusions have mostly irregular or rounded shapes, and some of the smaller inclusions are faceted (e.g. Fig. 10d).

Intensive parameters

Temperature and oxygen fugacity (Table 3) have been determined using the Fe–Ti oxide geothermobarometer from Ghiorso & Evans (2008); we discarded those oxide pairs that failed to meet the equilibrium criteria proposed by Bacon & Hirschmann (1988).

The calculated temperature for the Mamaku and Ohakuri Fe–Ti oxide pairs is between 740 and 820°C; log fO_2 (ΔNNO, where NNO is nickel–nickel oxide) ranges from −0·6 to 0·2, and is positively correlated with temperature (Fig. 12). In comparison with the other TVZ volcanic systems (Fig. 12), the Mamaku and Ohakuri mostly follow the trend of the 'dry and reduced' rhyolite types as characterized by Deering *et al.* (2010).

Crystallization conditions

The residence depth of the magma batches is essential to understanding their crystallization conditions, and the pre-eruptive reservoir geometry. We project the melt inclusion and bulk-rock compositions in the haplogranite Qz–Ab–Or ternary (Tuttle & Bowen, 1958; Holtz *et al.*, 1992). Data are corrected for their anorthite content using the method described by Blundy & Cashman (2001), and analyses with >1% normative corundum have been excluded (Fig. 13).

The projected melt inclusion and bulk pumice compositions for the Ohakuri Type 1 (Fig. 13a) overlap in the Qz–Ab–Or ternary, and plot in a very narrow range, indicating quasi-isobaric, nearly invariant (i.e. eutectoid) quartz-saturated crystallization under pressures around
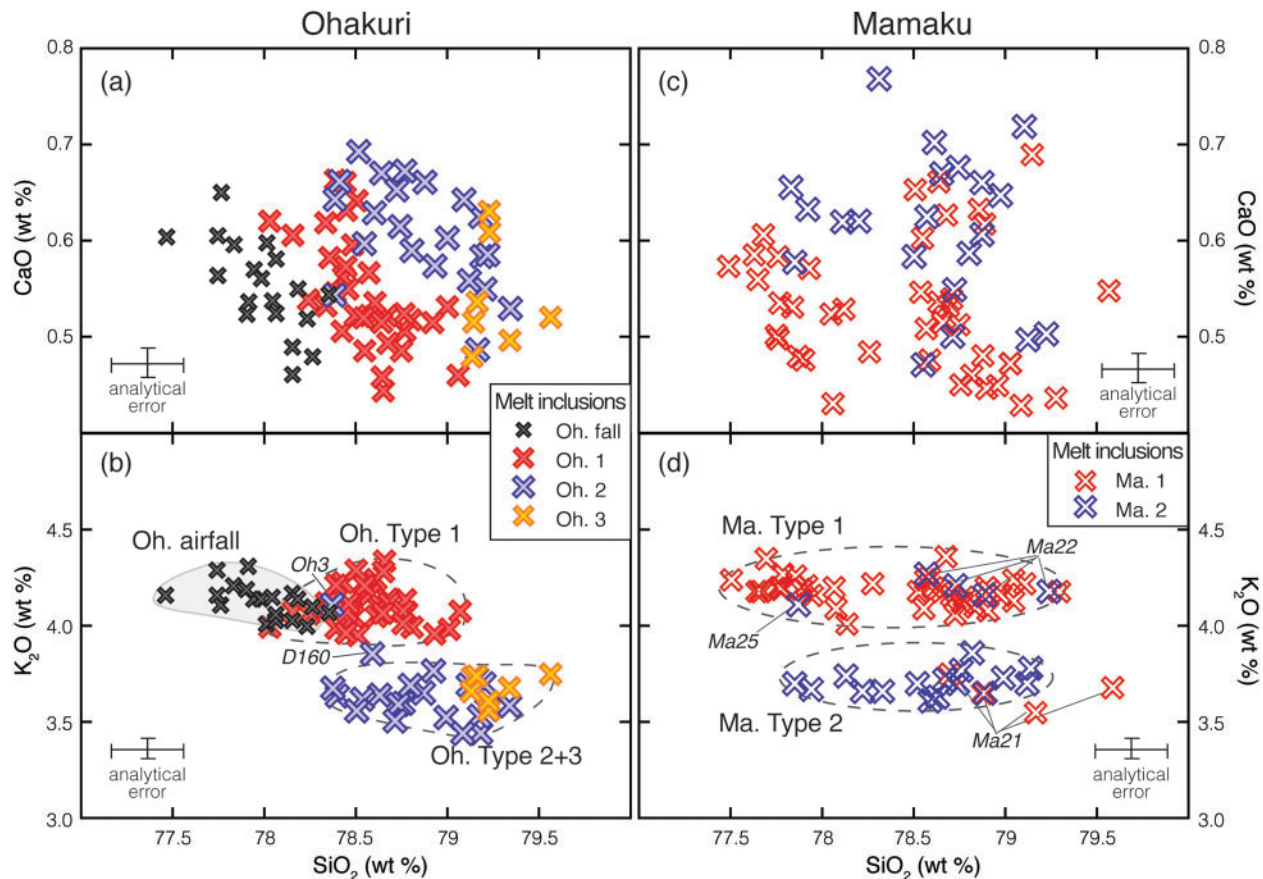
Fig. 7. Major element composition of the melt inclusions in the Ohakuri ignimbrite and fall deposit (a, b) and Mamaku ignimbrite (c, d).

50 MPa. It is noteworthy that the crystallinity in the Type 1 magma is <1 vol. % (Table 2). In contrast, Ohakuri Type 2 bulk compositions have lower normative quartz (Fig. 13a), and form an array toward the projected melt inclusion compositions. The compositional gap between the average bulk-rock and the melt inclusion composition is consistent with initial crystallization on the feldspar side (at quartz-undersaturated conditions), and may indicate late crystallization of quartz. The projected Mamaku melt inclusion compositions for Types 1 and 2 form an array in the Qz–Ab–Or ternary (Fig. 13b). This is interesting as it shows that even under conditions where quartz is saturated, the compositions evolve towards the Qz apex, suggestive of polybaric evolution. Similar compositional changes have been related to decompression crystallization (Blundy & Cashman, 2001), implying that magma decompression is slow enough for crystallization to continue.

To better constrain crystallization pressures we employed phase equilibria calculations using Rhyolite-MELTS (Gualda *et al.*, 2012a) to model crystallization pressures (Gualda & Ghiorso, 2014). Because melt inclusions represent melt in equilibrium with both quartz and

plagioclase (+ orthopyroxene and Fe–Ti oxides), they need to be saturated in both phases at their liquidus; given that the pressure effect on the slope of the saturation temperature is different for quartz and plagioclase, there is a cross-over in pressure–temperature space that corresponds to the crystallization conditions. In practice, the method consists of searching within a plausible range of pressures for the pressure at which the liquidus assemblage consists of quartz + plagioclase (Gualda & Ghiorso, 2013b, 2014). We use the melt inclusion compositions as input in Rhyolite-MELTS and run simulations at pressures of 25–400 MPa, in intervals of 25 MPa, under water-saturated conditions and oxygen fugacity fixed at NNO. Importantly, the resulting pressure estimates are insensitive to the assumption of water-saturation (Gualda & Ghiorso, 2013b, 2014). Details on the application of this geobarometer to TVZ rhyolites are beyond the scope of this study, and will be the topic of a separate study (Bégué *et al.*, in review).

Application of this method leads to estimated pressures that range from 60 to 130 MPa for the Mamaku ignimbrite (Fig. 14). These results are fairly consistent and do not
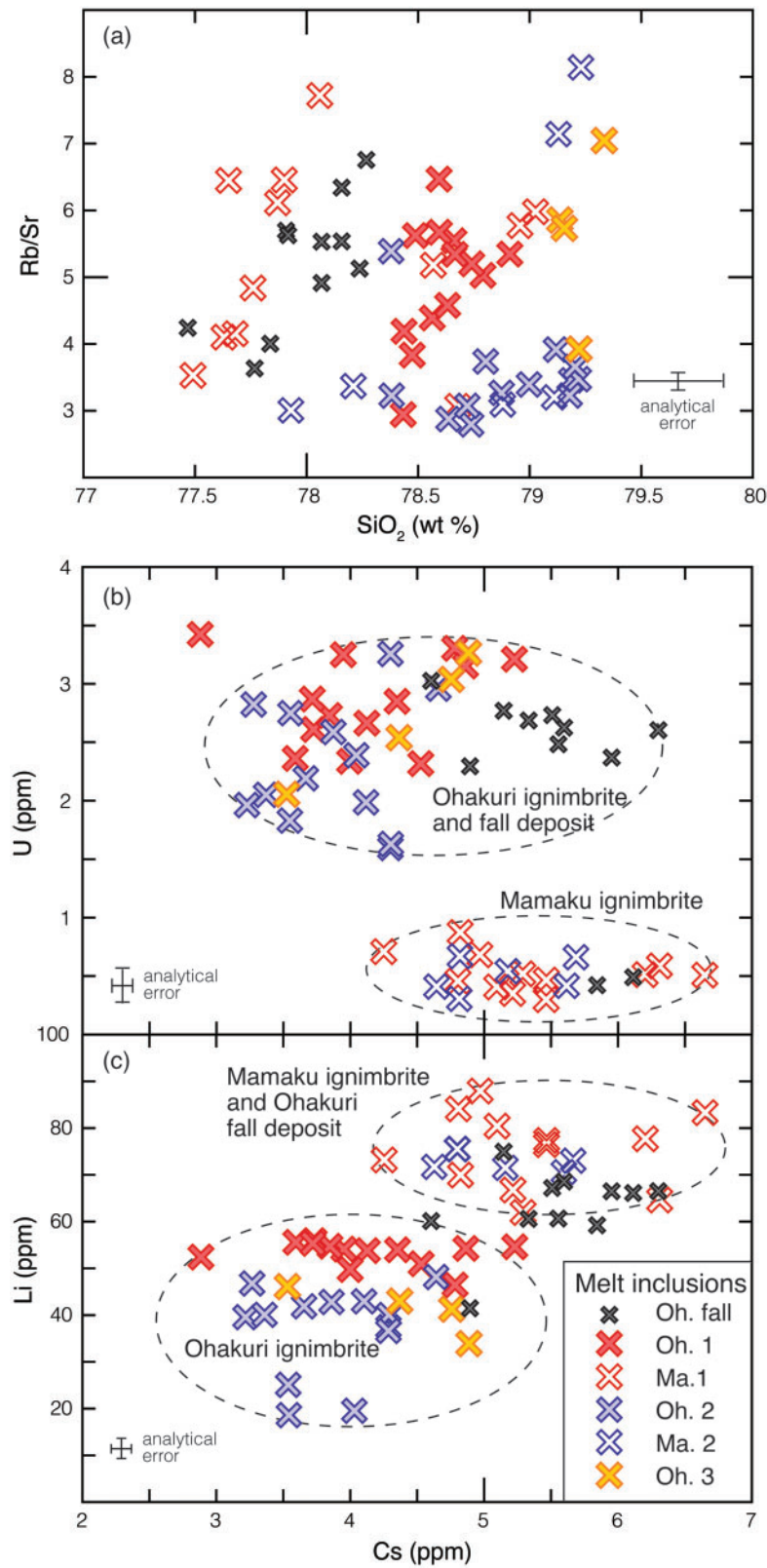
Fig. 8. Trace element composition of the melt inclusions in the Mamaku (open symbols), and Ohakuri (filled symbols) ignimbrites and the Ohakuri fall deposit; (a) SiO_2 vs Rb/Sr; (b) Cs vs U; (c) Cs vs Li.
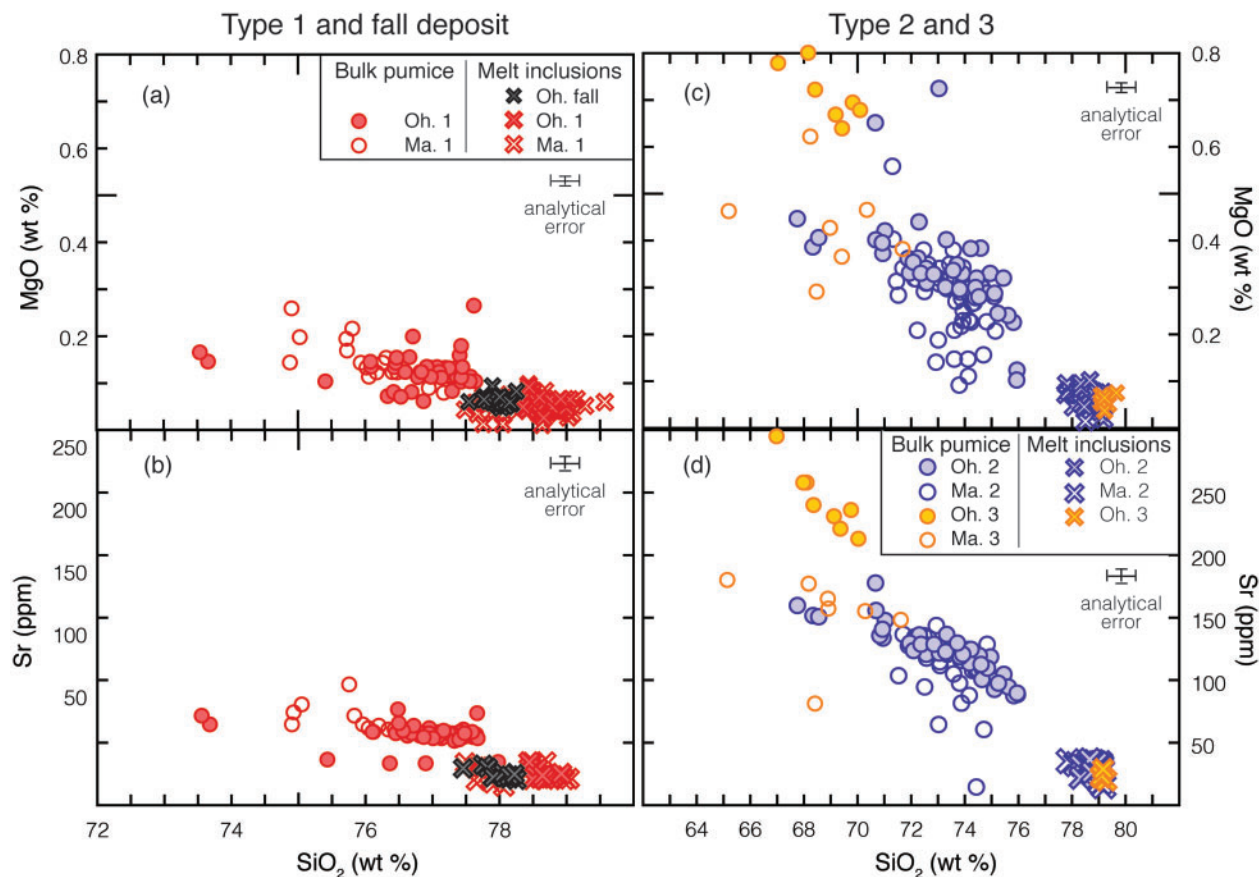
Fig. 9. Variation of MgO and Sr vs SiO$_2$ for the melt inclusions compared with the bulk pumice chemistry (Milner, 2001; Gravley, 2004) for Type 1 and Ohakuri fall deposit (a, b), and Types 2 and 3 (c, d); open symbols, Mamaku; filled symbols, Ohakuri.

seem to suggest polybaric crystallization of the Mamaku magma, at least within the level of uncertainty ($\sim$50 MPa, 2σ) as seems to be indicated by the Qz–Ab–Or ternary diagrams (Fig. 13b). The Ohakuri rhyolites yield lower pressure estimates, with values ranging between 30 and 50 MPa (Fig. 14). However, these calculations do not seem to be reliable, and only nine out of 65 melt inclusion analyses for the Ohakuri melts have a solution in the phase equilibria calculations, and should be treated as absolute minimum pressures. Nevertheless, the pressure range resulting from the rhyolite-MELTS geobarometer seems to agree reasonably well with the estimates in Fig. 13. The very high SiO$_2$ content (77–80 wt %) and the low An content of plagioclase (Fig. 3a) are also consistent with shallow storage pressures (Blundy & Cashman, 2001; Gualda & Ghiorso, 2013a). The estimated pressures are also in agreement with the pressures that have been suggested for other TVZ rhyolites based on H$_2$O–CO$_2$ solubilities in melt inclusions, 50–200 MPa for the Okataina Volcanic Center (Smith *et al.*, 2010; Johnson *et al.*, 2011), and 90–190 MPa for the Oruanui rhyolite (Liu *et al.*, 2006), although the lower end of these pressure ranges is considered to be related to degassing of the melt. These results reinforce the fact that the central TVZ magmas are stored in some of the shallowest magma reservoirs on Earth, which is suggested to be related to an exceptionally high heat flux from depth (Bibby *et al.*, 1995) and to the extensional tectonic regime.

DISCUSSION

This dataset of new and compiled compositions for bulk-rocks, minerals, matrix glasses and melt inclusions allows us to reconstruct the evolution of the magma types of the Mamaku and Ohakuri magmatic system from the parent magma source to the simultaneous eruptions. For the following discussion we will use the terminology of Miller *et al.* (2011) to distinguish between the magma chamber (i.e. the continuous zone where eruptible magma is present), the magma reservoir (i.e. all of the melt-bearing region, including magma chambers and crystal-rich, non-eruptible magma or mush), and the magmatic system (which encompasses the magma chamber and reservoir, as well as the solidified portion representing an active zone of magma transfer and storage).
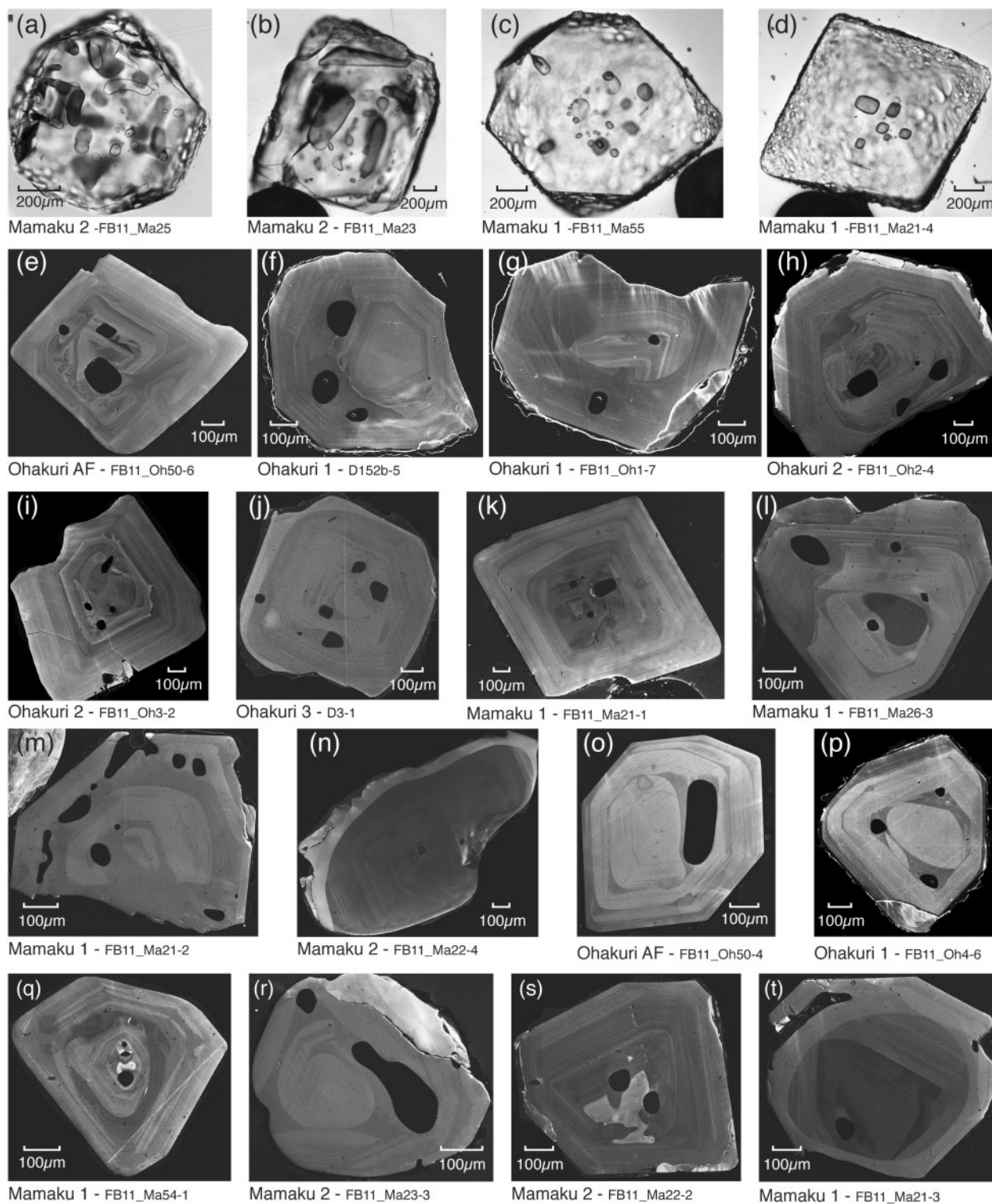
Fig. 10. (a–d) Photomicrographs in transmitted light of selected quartz crystals; (e–t) representative CL images of quartz crystals.
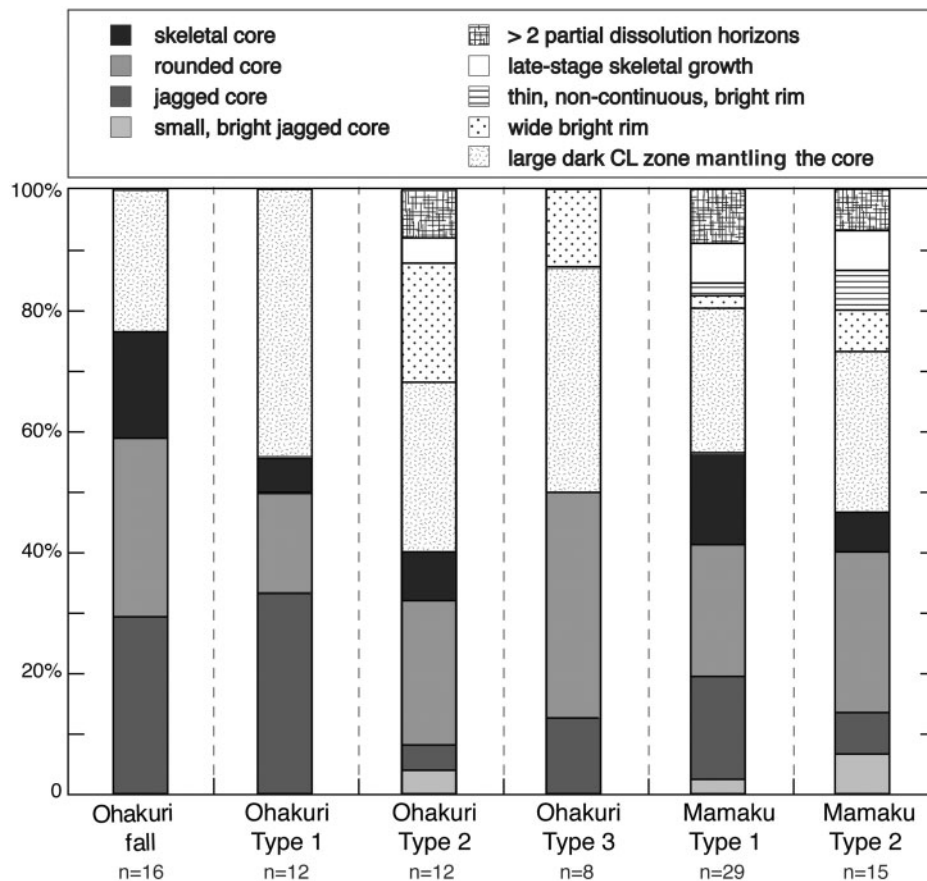
Fig. 11. Frequency of the CL zoning types identified for each pumice type of the Mamaku, and Ohakuri ignimbrites and the Ohakuri fall deposit. (See text for description of the zoning patterns.)

Rhyolite petrogenesis and magma reservoir geometry

Multiple stages of crustal assimilation and fractional crystallization processes (AFC) from a basaltic parent have been suggested in many studies to explain the origin of evolved magma compositions (e.g. Bachmann & Bergantz, 2004; Annen *et al.*, 2006; Hildreth & Wilson, 2007). To explain the presence of large volumes of crystal-poor silicic magma in the upper crust, current models appeal to the presence of a crystal-rich intermediate mush zone in the mid- to upper crust, which can be up to a few kilometres thick (Hildreth & Fierstein, 2000; Bachmann & Bergantz, 2004; Hildreth, 2004; Hildreth & Wilson, 2007; Deering *et al.*, 2011a). The interstitial melt from this crystalline mush represents the rhyolitic melt, and is extracted by a combination of processes (mainly hindered settling and/or compaction) to form crystal-poor high-silica chambers in the upper parts of the reservoirs (Bachmann & Bergantz, 2004). The optimal crystallinity window for efficient melt extraction from the mush is probably between ~50 and 70% crystals (Dufek & Bachmann, 2010). The longevity of the mush system in the

upper crust is maintained thermally by episodic heat and mass input from recharge of intermediate magma into the mush zone (Bachmann & Bergantz, 2004; Hildreth, 2004; Annen *et al.*, 2006; Hildreth & Wilson, 2007; Gelman *et al.*, 2013).

The 240 ka Mamaku and Ohakuri rhyolites are both 'dry-reducing' magmas (R2 rhyolite type, after Deering *et al.*, 2008, 2010), and show many similarities in their bulk-rock geochemistry, mineral assemblage (Table 2) and heterogeneity of pumice composition in their pyroclastic deposits. They also have similar ranges of oxygen fugacity and temperature (Fig. 12). Despite these similarities, there are also some differences. Orthopyroxene compositions in the Mamaku ignimbrite encompass a broader range compared with Ohakuri. In comparison with a larger TVZ mineral dataset (Deering *et al.*, 2010), the Ohakuri and most of the Mamaku pyroxenes plot in the range of the dry-reducing pyroxenes, as expected, but the high-En population of the Mamaku overlaps with the wet-oxidizing rhyolite end-member compositions. In the melt inclusion compositions, small differences in fluid-mobile elements are observed, with the Mamaku melt inclusions having
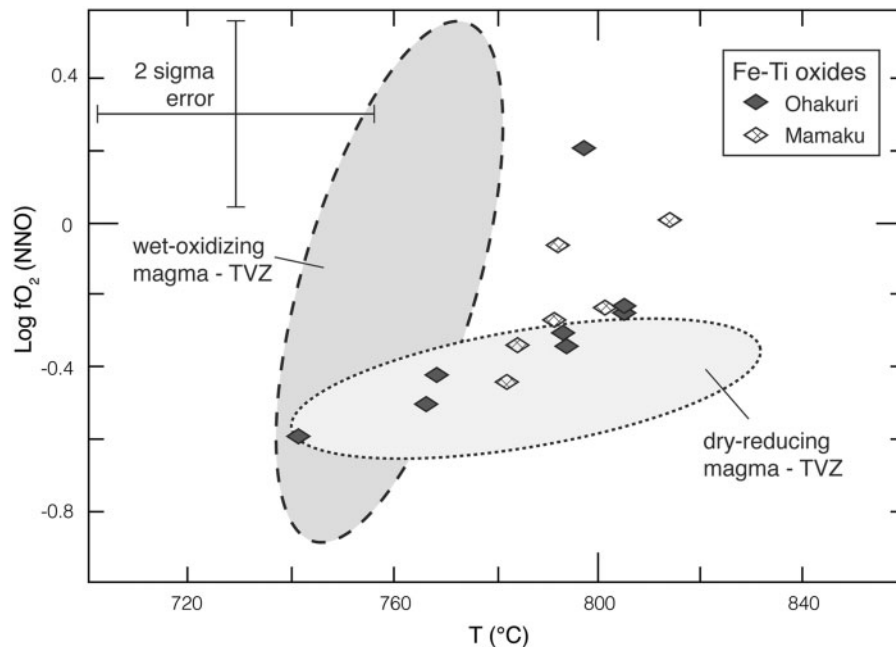
Fig. 12. Temperature vs fO_2 calculated for the Mamaku (open symbols) and Ohakuri (filled symbols); error bars represent $\pm 2\sigma$; grey shaded fields represent data for the 'dry-reducing' and the 'wet-oxidizing' rhyolites in the TVZ (after Deering *et al.*, 2010).

lower U, and higher Cs and Li contents (Fig. 8b and c). Other differences between the Mamaku and Ohakuri eruptive rocks have been previously observed (Gravley *et al.*, 2007), with differences in their plagioclase to quartz ratios (Table 2), bulk Zr concentration for the Type 2 magma. which has a broader range of variation in the Mamaku ignimbrite (i.e. overlaps with the Type 3 magma), and Rb/Sr ratio, which is more variable in Ohakuri Type 1 (Gravley *et al.*, 2007).

Despite these subtle compositional differences, the predominant geochemical similarities suggest that at a broader scale, the Ohakuri and Mamaku magmas are derived from a very similar source. Considering the current model for rhyolite petrogenesis, consisting of a mid-crustal mush zone, we infer extraction of the Mamaku and Ohakuri magmas from a common intermediate crystalline mush zone, extending between and beneath the Rotorua and Ohakuri calderas (Fig. 1). The low-crystallinity nature of these rhyolites and the absence of co-erupted intermediate magma compositions are in agreement with the presence of a crystal mush, which is relatively non-eruptible. Only rare andesitic 'blebs' have been found in the Mamaku and Ohakuri eruptive products, and no mingled or mixed composition pumices have been reported (Milner *et al.*, 2003; Gravley *et al.*, 2007). Considering the $\sim$450 km^2 horizontal extent of the above-mentioned common mush ($\sim$45 $\times$ 10 km; Fig. 1), hindered settling by $\sim$500 m would be sufficient to extract $\sim$225 km^3 of rhyolitic melt (after Bachmann & Bergantz, 2004), regardless of the total mush

thickness and the melt segregation process. This rough estimate of total melt produced is consistent with the suggested minimum erupted volume from the Mamaku and Ohakuri eruptions, but would also require the presence of magma beneath the area between the Rotorua and Ohakuri volcanic centres (Kapenga area). This has been suggested based on field evidence for the Ohakuri system, with magma (referred to as the Kapenga magma; Gravley, 2004) residing underneath the Kapenga area (Fig. 1), which migrated SW to the current location of the Ohakuri caldera (Gravley *et al.*, 2007).

This crystal mush can remain near the eutectic for extended periods of time (Huber *et al.*, 2010), especially if thermal rejuvenation by recharge occurs periodically (e.g. Bachmann & Bergantz, 2004; Annen, 2009; Gelman *et al.*, 2013). This is a likely scenario in the central TVZ during the period in question, as high mantle power is required to sustain magmatism associated with the $\sim$340–240 ka ignimbrite flare-up event (Best & Christiansen, 1991; de Silva & Gosnold, 2007; Gravley *et al.*, 2009, in preparation). A long-lived subterranean crystal mush, perturbed by episodic rejuvenation, has also been identified at other central TVZ magmatic systems, as evidenced by recent zircon geochronology work on rhyolites from the Okataina Volcanic Centre (Fig. 1a; Storm *et al.*, 2011). Local, minor heterogeneities in this mush zone probably persist owing to the high but slightly variable crystallinities and lack of large-scale convective homogenization (Dufek & Bachmann, 2010), and the melt extraction efficiency
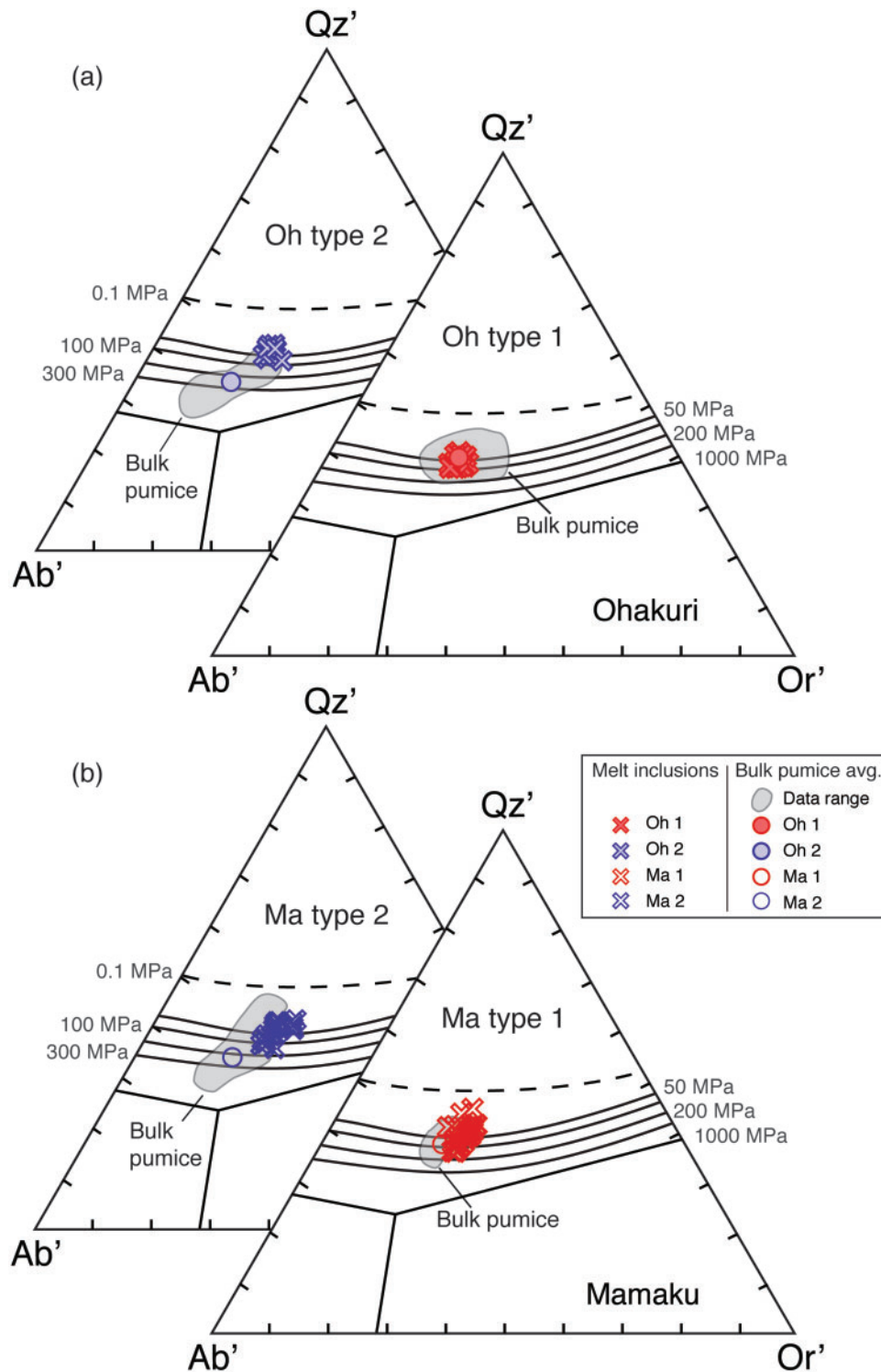
Fig. 13. Projection of melt inclusion and average bulk pumice compositions into the haplogranite Qz–Ab–Or ternary; correction for anorthite content after Blundy & Cashman (2001); (a) Ohakuri ignimbrite, Type 1 and 2; (b) Mamaku ignimbrite, Type 1 and 2. The grey shaded area represents the bulk pumice composition range. Ohakuri Type 3 data are not included here as the melt inclusions are not in equilibrium with the bulk melt composition.
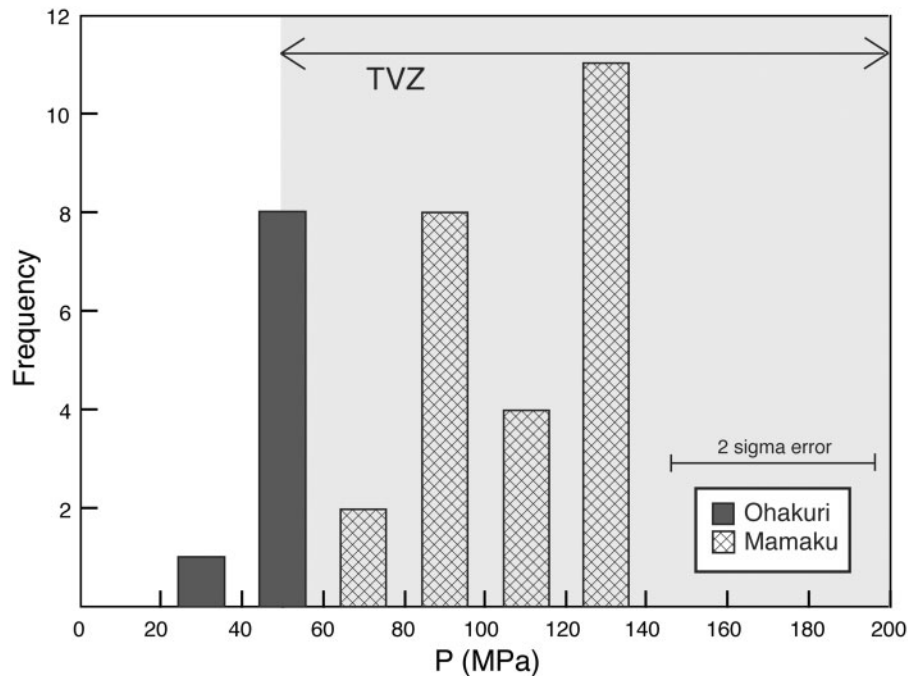
Fig. 14. Pressure vs frequency diagram for the Mamaku and Ohakuri ignimbrites showing the results of the phase equilibria calculations using Rhyolite-MELTS and the composition of quartz-hosted melt inclusions (method after Gualda & Ghiorso, 2014). These results represent absolute minimum pressures. Grey shaded field represents the pressure range calculated from H_2O–CO_2 solubilities for the Oruanui ignimbrite and the Okataina Volcanic Centre of the TVZ (after Liu *et al.*, 2006; Smith *et al.*, 2010; Johnson *et al.*, 2011).

may vary along a horizontally extensive mush. Local mush heterogeneities have also been suggested as the cause of geochemical variations for the smaller Okareka eruption (Okataina Volcanic Centre; Shane *et al.*, 2008). Similarly, we conclude that the compositional differences between the Mamaku and Ohakuri magmas are related to heterogeneities in the mush zone.

Rhyolite magma batches

In the scenario proposed above, the Mamaku and Ohakuri magmas were extracted from the same, locally heterogeneous, source reservoir, and they both are characterized by very similar variations in their pumice chemistry; in fact, we observe larger chemical differences between the magma types at a single centre than between the Ohakuri and Rotorua centres. Three distinct magma types are present in their respective ignimbrites, a less evolved dacitic to rhyodacitic Type 3 melt and two evolved, high-silica rhyolites, Types 2 and 1. In addition, the melt inclusions from these magma types also have distinct compositions (Figs 7 and 8a); however, they show a narrow range of SiO_2, which suggests similar crystallization conditions (Gualda & Ghiorso, 2013a). The bulk-rock and melt inclusion chemistry for Types 1 and 2 (Mamaku and Ohakuri) plot along the same liquid line of descent (Fig. 9), suggesting that the melt inclusions are in equilibrium with their respective bulk magma type. The lower MgO content in the melt inclusions compared with the

bulk-rock chemistry indicates that their entrapment occurred after the crystallization of some mafic minerals (Fig. 9a and c). The presence of a compositional gap between the bulk-rock and melt inclusion compositions for Types 2 and 3 of the Ohakuri and Type 2 for the Mamaku ignimbrites (Fig. 9c and d) further emphasizes that melt inclusions were entrapped late (i.e. quartz crystallized relatively late in the pre-eruptive history). For the Ohakuri ignimbrite, we also observe that Type 1 melt inclusions are present in only Type 1 pumice, and the same applies to Type 2 (Fig. 6c and f). This indicates that no discernible mixing between these two magma types occurred prior to eruption. For the Mamaku ignimbrite, some melt inclusions with Type 1 matrix glass have compositions similar to Type 2 magma and vice versa (Fig. 7d). However, this does not apply to all of the analysed melt inclusions from the same pumice, and the matrix glass compositions from the pumice clasts in question do not indicate any mixing prior to eruption.

In the most recent model proposed to explain the co-eruption of these chemically distinct bulk magma compositions for the Mamaku ignimbrite (Milner *et al.*, 2003), Type 3 magma represents the parental magma for the generation of Type 2, and consequently Type 1 magma through plagioclase fractionation. The result is a single, vertically zoned magma chamber, geochemically layered, with Type 3 magma being the deepest layer in the chamber and Type 1 the shallowest (Milner *et al.*, 2003). Similar models

of magma chambers fractionating *in situ* have been used in the past to explain heterogeneous pumice chemistry [e.g. Grizzly Peak Tuff, Colorado, USA (Fridrich & Mahood, 1987); Whakamaru ignimbrite, TVZ (Brown *et al.*, 1998)]. However, both the bulk-pumice and melt inclusion compositions for the Mamaku and Ohakuri ignimbrites are in disagreement with this model. Major and trace element compositions of the Type 2 and 1 melt inclusions plot along divergent trends (Figs 7 and 8a), and compositional gaps are often observed between the types; therefore, crystal fractionation is ruled out as a dominant process for the generation of Type 1 magma from Type 2 compositions. A similar argument has been made using Ohakuri bulk-rock compositions, which show that Rb and Sr in Type 2 and 1 plot along divergent linear trends (Fig. 2; Gravley *et al.*, 2007).

A model involving separate and chemically distinct magma batches has been suggested as an alternative to the layered magma chamber model at large silicic systems elsewhere (e.g. Cambray *et al.*, 1995; Shane *et al.*, 2007, 2008; Gualda & Ghiorso, 2013b). The melt is extracted incrementally from the mush zone, and may or may not amalgamate in a large magma chamber. This model accounts well for the distinct compositions of the Ohakuri Type 1 and 2, as each melt batch is extracted separately. Moreover, it seems that very limited mixing between the magma types occurred, which would be indicative of a lack of direct interaction among the distinct magma batches. The coincidence of the different magma types at the same stratigraphic level is considered to reflect simultaneous eruption of all magma batches, which would have to be very close to each other in the upper crust. A similar model of isolated magma batches has also been proposed for other systems [e.g. Rotoiti–Earthquake Flat, Okataina Volcanic Center (Charlier *et al.*, 2003); Batur Volcanic Field, Indonesia (Reubi & Nicholls, 2005); Snake River Plain, USA (Ellis & Wolff, 2012)]. The evidence for multiple magma batches is less obvious in the bulk compositions of the Mamaku ignimbrite (Fig. 2), but the melt inclusion compositions support separate batches (Figs 7 and 8a). The outliers among the Mamaku melt inclusions are not indicative of mixing between Types 1 and 2, as the compositional differences are not consistent for all analysed elements, and throughout the pumice clasts. These outliers could represent quartz grains of xeno- or antecrystic origin, relics of the magmatic reservoir that fed older eruptions from the overlapping Kapenga caldera (Fig. 1; i.e. ~275 ka Pokai ignimbrite), or assimilation of the largely crystallized margins of the reservoir. From the CL images, we identify a distinct core zone in the majority of the quartz grains (Figs 10 and 11). With the available data, we cannot assign an origin to these cores; however, an inherited origin is consistent with the variability in CL-zoning of quartz cores in crystals from the same pumice clast.

Type 3 melt inclusions from the Ohakuri ignimbrite are the most evolved (up to ~80 wt % SiO_2), in contrast to the bulk composition, which is the least evolved (~68 wt % SiO_2). This melt type represents only a very small volume compared with Types 1 and 2, and it also has the highest crystallinity, ~15 vol. % (Table 1), which could be indicative of a crystal accumulation zone. However, there is no chemical evidence that would directly support this, as bulk concentrations of chemical tracers for accumulation zones [i.e. Zr, Rb, and Ba (Table 1); Kennedy & Stix, 2007; Deering & Bachmann, 2010] are similar for Type 2 and 3 magmas. Regarding the differences in SiO_2 content between the bulk pumice and melt inclusions and the crystallinity, it is also very unlikely that the quartz is in equilibrium with the melt, suggesting that they could be of antecrystic origin. Incorporation of the crystallized margins of the reservoir [see Brown *et al.* (1998) for a number of examples of plutonic lithic fragments; also Shane *et al.* (2012)] could account for the presence of quartz crystals with high-silica rhyolite melt inclusions, as co-erupted granodiorite lithic fragments are found within the Ohakuri ignimbrite (D. Gravley, personal communication, 2012). Another plausible explanation for the presence of these high-silica melt inclusions in the Type 3 quartz is mixing of a rhyodacitic magma with a rhyolitic melt. The Type 3 melt inclusions are chemically very similar to the Type 2 inclusions, which could indicate some degree of interaction with the Type 2 melt batch. However, the distinct Rb/Sr ratio of the Type 3 melt inclusions compared with the Type 2 (Fig. 8a) and the absence of a clear mixing trend in the bulk-rock chemistry (Gravley *et al.*, 2007) between those two types suggest that interaction with a different rhyolitic melt is more likely (i.e. a melt that was not erupted with the Ohakuri).

The Ohakuri fall deposit, sourced from or adjacent to the Ohakuri caldera (Gravley *et al.*, 2007), is the first eruptive unit, and its melt inclusion chemistry is very similar to a Type 1 magma (Figs 7 and 8). However, it seems to share more geochemical characteristics with a Mamaku melt, and shows the same enrichment in Cs and Li (Fig. 8b and c). Enrichment in fluid-mobile elements is common in early erupted material such as the Ohakuri fall deposit, owing to volatile fluxing from degassing magma (e.g. Berlo *et al.*, 2004). However, here we have evidence to suggest that the fall deposit is a separate batch from the other Ohakuri magmas, as differences in other trace elements apart from the fluid-mobile elements can be observed, and from pressure estimates the melts from the fall deposit seem to reside at slightly greater depth compared with the Ohakuri magmas (Bégué *et al.*, in preparation). The relationship between the Ohakuri fall deposit and the Mamaku and Ohakuri magmas is not well understood and remains to be explored. From current knowledge of the Mamaku–Ohakuri, and other central TVZ magma

systems, however, tapping into a magma chamber that is tens of kilometres away from the vent location and lateral magma movements may be a plausible explanation for these chemical similarities between the Ohakuri fall deposit and the Mamaku magmas. With the data available at present, this remains speculative, and for now the fall deposit is represented as a separate magma batch residing close to the Ohakuri centre. Further work will be focused around this problem.

Pre-eruptive magmatic system

A schematic model for the Mamaku and Ohakuri magmatic system takes into consideration all the above observations in the geochemical data and volcano-tectonic events described by Gravley et al. (2007) (Fig. 15). A continuous intermediate mush zone, which extends beneath the Ohakuri and Rotorua areas, is the source of the distinct magma batches involved in the paired eruption. Of the multiple magma batches, at least four are spatially isolated, as no mixing is observed between the Type 1 and Type 2 Ohakuri and Mamaku magmas. The much smaller Ohakuri Type 3 and fall deposit magma batches are also represented, although their magmatic history is not well constrained. As suggested above, the Type 3 magma composition may have involved mixing of a rhyodacite with a rhyolite or some previously emplaced granitic material, indicated by the melt composition trapped in the quartz crystals.

The extensional tectonic regime of the central TVZ, with its profound interrelationship between magmatism, tectonics, and volcanism (Wilson et al., 2009; Rowland et al., 2010) is probably not the most favourable environment for the establishment of longer-lived magma chambers. Lateral magma migration has been described in the literature as a result of this unstable crustal environment for the Oruanui eruption (Allan et al., 2012), and is also suggested here for the Ohakuri eruption. Field evidence shows that syn-eruptive subsidence of a $40\,km^2$ area in the Kapenga region and formation of the Horohoro fault scarp (Fig. 1b) occurred during the Ohakuri eruption; this is suggested to reflect magma residing underneath the Kapenga area and migrating SW to the current location of the Ohakuri caldera (Gravley et al., 2007). The discrete magma batch model suggested here is in agreement with the structural evidence for lateral magma migration, as one of the magma batches may have resided beneath the Kapenga area. Another line of evidence is the compositional and isotopic similarities between the Ohakuri rhyolite and the Horohoro dome (Fig. 2; Deering et al., 2008), which is located on the western margin of the Kapenga caldera (Fig. 1b). This dome erupted prior to, and was subsequently faulted in response to, lateral migration of the magma that fed the Ohakuri ignimbrite eruption (Gravley et al., 2007). However, there is currently not enough geological evidence to identify which magma type

laterally migrated from beneath the Kapenga area to its eruption site. The random distribution of the magma types throughout the eruptive deposits is indicative of simultaneous evacuation of the various magma batches during the eruption, and may be associated with eruptive processes and styles of caldera collapse (e.g. Kennedy et al., 2008). The estimated pressures yield similar results (within the error) for the various magma types, corresponding to a depth of $\sim$4 km (using a crustal density of $2{\cdot}7\,g\,cm^{-3}$), which would be concordant with a model of laterally juxtaposed magma batches in the upper crust.

A unique aspect of the Rotorua–Ohakuri magmatic system is that almost chemically identical Type 1 and Type 2 magmas were extracted at two different locations. Timing of melt extraction from the common crystal mush may play an important role in producing the same rhyolites beneath the Rotorua and the Ohakuri volcanic centres, and the Type 1 and Type 2 magmas could represent the products of two distinct extraction events. This raises the important question of the driving mechanism for melt extraction and the available time frame to assemble $>$245 km^3 of crystal-poor rhyolitic melt.

Extraction timescales and processes

The timescales for rhyolitic melt extraction and crystallization within the extracted melt have been estimated to be faster (e.g. Wilson & Charlier, 2009; Gualda et al., 2012b) than suggested by models of melt segregation from an intermediate mush by hindered settling (e.g. Bachmann & Bergantz, 2004). The $\sim$275 $\pm$10 ka Pokai ignimbrite lies stratigraphically beneath the Ohakuri and the Mamaku ignimbrites, with a well-developed paleosol separating the units (Gravley et al., 2007). The Pokai magma was sourced from the Kapenga caldera (Fig. 1; Karhunen, 1993), within the same area in which later, during the paired Mamaku–Ohakuri event, syn-volcanic subsidence occurred (Figs 1 and 15). This subsidence suggests the presence of magma during the $\sim$240 ka event in the same region in which the Pokai magma resided (Gravley et al., 2007), which leaves between $\sim$15 and 55 kyr to generate and extract the crystal-poor rhyolite erupted during the Mamaku and Ohakuri events in the region of the Kapenga caldera. The rhyolites feeding these eruptions probably shared the same intermediate mush. This inference is supported by that fact that the Pokai rhyolite is geochemically very similar to the Mamaku and Ohakuri magmas; it is a 'dry-reducing' magma (Deering et al., 2008), it has the same anhydrous mineral assemblage and similar bulk-rock composition (Fig. 2; Karhunen, 1993; Gravley, 2004), which is supportive of a common mush zone.

After eruption of the Pokai ignimbrite, rejuvenation (reheating, remelting and melt extraction) of the intermediate mush occurred, and extraction could resume and form new pockets of crystal-poor melt in this area to form the
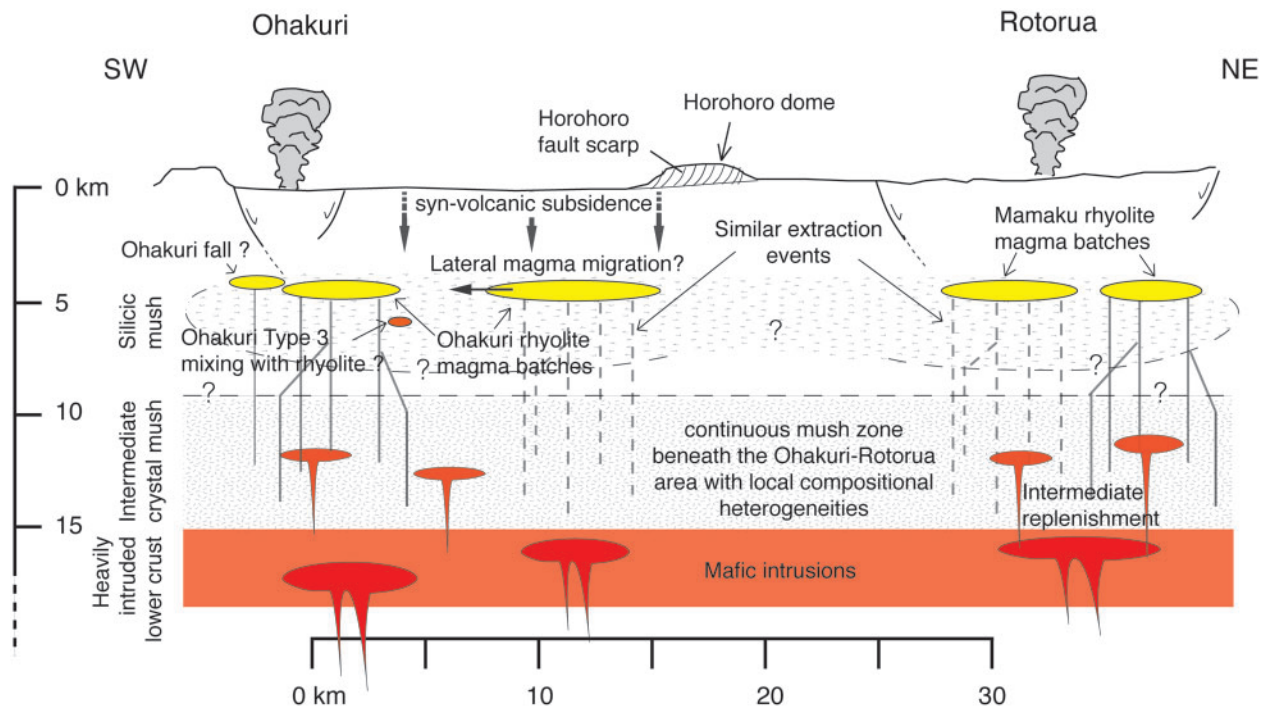
Fig. 15. Schematic model of the Rotorua and Ohakuri magma systems based on inferred pre-eruptive conditions (this study) and geomorphological reconstructions (Gravley *et al.*, 2007). Heterogeneous pumice clast chemistry in the eruptive rocks is suggested to reflect multiple magma batches extracted from the same source (i.e. intermediate mush zone). Extraction conditions for the Type 1 magma are suggested to be very similar between the two eruptive centres (also for the Type 2 magma); no mixing of these magma batches occurred prior to eruption. (Scale and relative volumes are approximate.)

Mamaku and Ohakuri magma batches. The presence of antecrysts in the Mamaku and Ohakuri melts has been suggested to explain the compositional outliers in the melt inclusion data, and the lack of equilibrium between melt inclusion and bulk-rock compositions for Type 3. Furthermore, CL imaging has revealed the presence of inherited core in most of the crystals. These aspects are evidence for the process of reheating, remelting and melt extraction, which probably remobilizes some existing melt and also crystals.

Crystal–melt segregation and melt extraction mechanisms are suggested to be a combination of hindered settling, micro-settling and compaction of crystals in the mush zone; however, grain size and porosity are the important parameters dictating the melt segregation timescales (Bachmann & Berganz, 2004). These timescales can be relatively fast, especially if hindered settling is the dominant process, and have been suggested to be 10^4–10^5 years for the extraction of $\sim$500 km^3 of rhyolite (Bachmann & Berganz, 2004). Wilson & Charlier (2009), however, provided evidence for much shorter timescales of around $\sim$3000 years for melt accumulation of the $\sim$530 km^3 Oruanui magma (TVZ); such timescales are supported by the work of Gualda *et al.* (2012*b*) on the Bishop Tuff. These timescales for melt accumulation are within the available timeframe for the Mamaku and

Ohakuri rhyolites. However, if we consider that the Type 1 and Type 2 magmas represent two temporally distinct melt extraction episodes, these would have to be in rapid succession, suggesting very efficient melt extraction from the crystal mush, and, consequently, efficient rejuvenation of this mush. In the central TVZ where tectonism and magmatism are closely linked (Wilson *et al.*, 2009; Rowland *et al.*, 2010) it is possible that regional-scale tectonism may have played an important role as an additional mechanism accelerating the melt extraction process from the crystal mush. The short time window to extract the melt could also be one of the reasons for the isolated magma batches, suggesting that there was not enough time for amalgamation of the different batches into either a single large magma body or two separate magma chambers located below the Rotorua and Ohakuri centres.

Eruption triggers

The Mamaku and Ohakuri eruptive events are thought to have occurred over the course of several days or weeks (Gravley *et al.*, 2007). The initial event resulted in the fall deposit sourced from the Ohakuri region, followed by the Mamaku pyroclastic flows, and the Ohakuri flows, each containing three distinct magma types (Gravley *et al.*, 2007). This leads to the question of what triggered this sequence of eruptive events and allowed the almost

synchronous eruption of several distinct magma types. The quest to understand the triggers of such large, silicic ignimbrite-forming eruptions has been frequently addressed in the literature (e.g. Sparks *et al.*, 1977; Pallister *et al.*, 1992; Manga & Brodsky, 2006; de Silva *et al.*, 2008). It is often suggested that destabilization of the magma chamber is induced by overpressurization, either by magmatic input into the chamber, or by an external trigger (e.g. depressurization, or change of regional stress regime). The internal pressure of a magma chamber can be increased by either directly increasing its volume by liquid mass addition, or indirectly, by increasing the volatile content as a more mafic magma input quenches and exsolves a vapour phase (e.g. Sparks *et al.*, 1977; Blake, 1981; Pallister *et al.*, 1992; Folch & Martí, 1998).

Quartz CL has been used in a number of recent studies to identify the involvement of mafic and felsic magma replenishment where direct evidence of mass addition is otherwise cryptic (e.g. Matthews *et al.*, 2011; Wilcock *et al.*, 2012). The CL zoning is used as a proxy for variations in Ti concentration in quartz (Wark & Spear, 2005), and crystallization temperature by virtue of the Ti-in-quartz thermometer (Wark & Watson, 2006). Mafic input is suggested to be responsible for the occurrence of bright rims that form sharp contacts along, or truncate, interior zones in the quartz crystals (reflecting an increase in Ti and temperature; Wark *et al.*, 2007; Wiebe *et al.*, 2007). Quartz CL in the Mamaku and Ohakuri eruptive products does not record crystallization of quartz crystals at uniformly higher temperature conditions prior to eruption. Bright CL rims are present in less than 10% of the imaged quartz (Fig. 11), and, furthermore, these bright rims are not systematically present throughout the investigated pumice clasts (i.e. quartz crystals in a single pumice clast do not all have bright rims). In a crystal-poor magmatic system such as the Ohakuri–Mamaku, heat transfer through single magma batches would have been rapid and should be recorded in a high proportion of the quartz phenocrysts. The origin of the rare bright CL rims thus remains unclear, other than that they may represent relicts from a magma reservoir that fed previous eruption.

In comparison with the quartz zoning, plagioclase crystals only exhibit normal zoning with regard to An, which indicates that they do not record the addition of a more mafic magma, nor an increase in temperature during their crystallization history. Despite the presence of rare mafic blebs, described by Milner *et al.* (2003) and Gravley *et al.* (2007), no basalt co-erupted with either the Mamaku or Ohakuri eruptions, unlike in other central TVZ eruptions where mafic input is the suggested trigger. For these latter eruptions basaltic clasts and/or mingling and mixing has been directly observed in the pyroclastic deposits (e.g. Kaharoa eruption, Leonard *et al.*, 2002; Whakamaru eruption, Brown *et al.*, 1998; Matthews *et al.*,

2011; Matahina eruption, Deering *et al.*, 2011*b*). Consequently, we consider a shallow mafic injection trigger unlikely for the Mamaku–Ohakuri eruptions.

Another way to trigger an eruption is to externally induce eruption by depressurization of the magma chamber or by changing the orientation of the stress field (i.e. tectonic control). Close relationships between volcanic eruptions and tectonics are a controversial topic, although there are examples of recent eruptions directly following large earthquakes [e.g. the 1960 fissure eruption after an M 9·5 earthquake in Chile (Lara *et al.*, 2004); the 2004–2005 M >8·5 earthquake series preceding the eruption of the Talang volcano, Indonesia (Walter & Amelung, 2007)]. An external, tectonic trigger has also been suggested for the ∼5 Ma Atana eruption, Central Andes, as indicated by geochemistry, caldera geometry and regional faulting (Lindsay *et al.*, 2001). Conversely, volcanic eruptions can reactivate regional faults (e.g. the 6·5 ka Kikai caldera eruption triggered two large earthquakes in southern Kyushu, Japan; Naruo & Kobayashi, 2002). These examples are all in subduction-related tectonic arc settings; however, for the TVZ, which is a 'rifted' arc, it may be appropriate to also compare with examples from volcanic regions undergoing high rates of extension.

In other continental rift settings, close associations between regional tectonism and volcanism have frequently been observed [e.g. coupled earthquake swarm and volcanism during the 2007 Oldoinyo Lengai eruption in the East African Rift (Baer *et al.*, 2008)], and silicic volcanism has also been suggested to be a precursor event for rift segment propagation events (e.g. Afar triple point; Lahitte *et al.*, 2003). In the TVZ several studies have described that close relationship, as well as the important controls exerted by regional tectonics on caldera structure and geometry (e.g. Cole *et al.*, 2010; Seebeck *et al.*, 2010). Furthermore, it has been suggested that an extensional tectonic regime was related to lateral magma movements in the shallow crust during the Oruanui super-eruption (Taupo Volcanic Centre; Allan *et al.*, 2012). The paired Rotoiti and Earthquake Flat eruptions is another example in the TVZ where regional tectonic adjustments related to caldera collapse associated with the Rotoiti eruption potentially triggered the Earthquake Flat eruption (Charlier *et al.*, 2003).

For the Mamaku and Ohakuri paired event, a structural link between the two calderas has been established, and the caldera geometries are related to regional faults (Milner *et al.*, 2002; Gravley *et al.*, 2007; Ashwell *et al.*, 2013). The Rotorua caldera shows a complex geometry where regional faults and magma withdrawal have interacted to generate complex collapse-style morphologies (down-sag, trapdoor and piecemeal; Milner *et al.*, 2002; Ashwell *et al.*, 2013). In the Ohakuri–Rotorua area, linked eruption-related regional faulting has also been identified (Gravley *et al.*, 2007), and lateral magma withdrawal

associated with the Ohakuri eruption is linked to collateral subsidence of a large area (Gravley *et al.*, 2007). Furthermore, the Mamaku and Ohakuri ignimbrites represent the last pulse of the ignimbrite flare-up (~340–240 ka), and this is suggested to coincide with a period of accelerated rifting (Gravley *et al.*, 2009, in preparation). Therefore, in the absence of evidence for mafic magma injections, an external tectonic eruption trigger is possible and this may in turn have set off a cascading sequence of subsurface magma batch linkage and eruption. We suggest here that reactivation and amalgamation of fault segments was associated with the evacuation of >245 km^3 of rhyolitic magma from two different locations, lateral migration of magma, formation of calderas and a collateral volcano-tectonic depression, all in a very short time period.

CONCLUSIONS

New melt inclusion and matrix glass data have been combined with existing bulk-rock and mineral data, to retrace the evolution of the Mamaku and Ohakuri magmatic systems associated with paired eruptions and two caldera collapses in the central TVZ. Both volcanic centres erupted chemically distinct magma types, which are present in both centres. On the basis of this comprehensive geochemical analysis, we show the following.

(1) The Rotorua–Ohakuri magmatism involved at least five magma batches, extracted from the same source reservoir (a continuous intermediate mush zone beneath the area).

(2) At least four of these magma batches were isolated from each other in the upper crust and evolved separately until eruption, as no mixing and mingling between these magma types has been identified.

(3) Minor geochemical differences in the batches are probably associated with different extraction conditions of the rhyolitic melt from a slightly heterogeneous intermediate mush zone.

(4) The similar magma types at the Ohakuri and the Rotorua caldera centres could be linked to parallel extraction conditions, and regional tectonics may have accelerated the extraction mechanism.

(5) Lack of evidence in melt compositions for mafic recharge prior to eruption, and from quartz cathodoluminescence imaging, suggests that a magmatic input is unlikely to be the eruption trigger. However, tectonic activity, which was previously suggested as a potential trigger (Gravley *et al.*, 2007), could be an efficient way to activate these isolated magma batches. The evacuation of one magma batch could adjust the local stress field sufficiently to trigger simultaneous eruption of an adjacent melt batch.

(6) Collateral subsidence features between the calderas, identified by detailed surface mapping (Gravley *et al.*,

2007), suggest lateral magma withdrawal, which is in good agreement with the model of juxtaposed small magma chambers in the upper crust.

Recent studies of major caldera-forming eruptions in the central TVZ have appealed to a model involving multiple magma batches, which seems to work well with the dynamic extensional tectonic regime. It is noteworthy here that the TVZ provides exceptional spatial and temporal resolution, allowing good correlation between surface features, geochemistry, and geochronology of the deposits. Without detailed fieldwork and a comprehensive geochemical evaluation at the crystal scale, the Mamaku and Ohakuri events might have been regarded as a single, large eruption associated with a caldera collapse encompassing the Rotorua, Kapenga and Ohakuri area [~450 km^2; compare Valles Caldera, 434 ± 2 km^2 and Long Valley, 350 ± 5 km^2 (e.g. Geyer & Martí, 2008)]. From this study, we suggest that the tectonically triggered eruption of a single, small magma chamber can in turn trigger additional eruptions through fault linkages between one or more small magma chambers, and lead to an otherwise unexpected, more catastrophic event. These results have important implications for hazard identification and risk assessment in active volcanic regions that host large calderas. In addition, the evidence for these rhyolitic magma batches being especially shallow could be important to volcanic monitoring and recognizing signs of caldera unrest.

SUPPLEMENTARY DATA

Supplementary data for this paper are available at *Journal of Petrology* online.

REFERENCES

Allan, A. S. R., Wilson, C. J. N., Millet, M.-A. & Wysoczanski, R. J. (2012). The invisible hand: Tectonic triggering and modulation of a rhyolitic supereruption. *Geology* **40**, 563–566.

Annen, C. (2009). From plutons to magma chambers: Thermal constraints on the accumulation of eruptible silicic magma in the upper crust. *Earth and Planetary Science Letters* **284**, 409–416.

Annen, C., Blundy, J. D. & Sparks, R. S. J. (2006). The genesis of intermediate and silicic magmas in deep crustal hot zones. *Journal of Petrology* **47**, 505–539.

Ashwell, P. A., Kennedy, B. M., Gravley, D. M., von Aulock, F. W. & Cole, J. W. (2013). Insights into caldera and regional structures and magma body distribution from lava domes at Rotorua Caldera, New Zealand. *Journal of Volcanology and Geothermal Research* **258**, 87–202.

Bachmann, O. & Bergantz, G. W. (2004). On the origin of crystal-poor rhyolites: extracted from batholithic crystal mushes. *Journal of Petrology* **45**, 1565–1582.

Bacon, C. R. & Druitt, T. H. (1988). Compositional evolution of the zoned calcalkaline magma chamber of Mount Mazama, Crater Lake, Oregon. *Contributions to Mineralogy and Petrology* **98**, 224–256.

Bacon, C. R. & Hirschmann, M. M. (1988). Mg/Mn partitioning as a test for equilibrium between coexisting Fe–Ti oxides. *American Mineralogist* **73**, 57–61.

Baer, G., Hamiel, Y., Shamir, G. & Nof, R. (2008). Evolution of a magma-driven earthquake swarm and triggering of the nearby Oldoinyo Lengai eruption, as resolved by InSAR, ground observations and elastic modeling, East African Rift, 2007. *Earth and Planetary Science Letters* **272**, 339–352.

Berlo, K., Blundy, J., Turner, S., Cashman, K., Hawkesworth, C. & Black, S. (2004). Geochemical precursors to volcanic activity at Mount St. Helens, USA. *Science* **306**, 1167–1169.

Bégué, F., Gualda, G. A. R., Ghiorso, M. S., Pamukcu, A. S., Kennedy, B. M., Gravley, D. M., Deering, C. D. & Chambefort, I. (in review). Phase-equilibrium geobarometers for silicic rocks based on rhyolite-MELTS. Part 2: Application to Taupo Volcanic Zone rhyolites. *Contributions to Mineralogy and Petrology*.

Best, M. G. & Christiansen, E. H. (1991). Limited extension during peak Tertiary volcanism, Great Basin of Nevada and Utah. *Journal of Geophysical Research* **B8**, 13509–13528.

Bibby, H. M., Caldwell, T. G., Davey, F. J. & Webb, T. H. (1995). Geophysical evidence on the structure of the Taupo Volcanic Zone and its hydrothermal circulation. *Journal of Volcanology and Geothermal Research* **68**, 29–58.

Blake, S. (1981). Volcanism and the dynamics of open magma chambers. *Nature* **289**, 783–785.

Blundy, J. & Cashman, K. (2001). Ascent-driven crystallisation of dacite magmas at Mount St Helens, 1980–1986. *Contributions to Mineralogy and Petrology* **140**, 631–650.

Brown, S. J. A., Burt, R. M., Cole, J. W., Krippner, S. J. P., Price, R. C. & Cartwright, I. (1998). Plutonic lithics in ignimbrites of Taupo Volcanic Zone, New Zealand; sources and conditions of crystallisation. *Chemical Geology* **148**, 21–41.

Cambray, F. W., Vogel, T. A. & Mills, J. G. J. (1995). Origin of compositional heterogeneities in tuffs of the Timber Mountain Group: The relationship between magma batches and magma transfer and emplacement in an extensional environment. *Journal of Geophysical Research* **100**, 15793–15805.

Cerling, T. E., Brown, F. H. & Bowman, J. R. (1985). Low-temperature alteration of volcanic glass: hydration, Na, K, ^{18}O and Ar mobility. *Chemical Geology* **52**, 281–293.

Charlier, B. L. A., Peate, D. W., Wilson, C. J. N., Lowenstern, J. B., Storey, M. & Brown, S. J. A. (2003). Crystallisation ages in coeval silicic magma bodies: ^{238}U–^{230}Th disequilibrium evidence from the Rotoiti and Earthquake Flat eruption deposits, Taupo Volcanic Zone, New Zealand. *Earth and Planetary Science Letters* **206**, 441–457.

Cole, J. W., Spinks, K. D., Deering, C. D., Nairn, I. A. & Leonard, G. S. (2010). Volcanic and structural evolution of the Okataina Volcanic Centre; dominantly silicic volcanism associated with the Taupo Rift, New Zealand. *Journal of Volcanology and Geothermal Research* **190**, 123–135.

Deering, C. D. & Bachmann, O. (2010). Trace element indicators of crystal accumulation in silicic igneous rocks. *Earth and Planetary Science Letters* **297**, 324–331.

Deering, C. D., Cole, J. W. & Vogel, T. A. (2008). A rhyolite compositional continuum governed by lower crustal source conditions in the Taupo Volcanic Zone, New Zealand. *Journal of Petrology* **49**, 2245–2276.

Deering, C. D., Gravley, D. M., Vogel, T. A., Cole, J. W. & Leonard, G. S. (2010). Origins of cold-wet-oxidizing to hot-dry-reducing rhyolite magma cycles and distribution in the Taupo Volcanic Zone, New Zealand. *Contributions to Mineralogy and Petrology* **160**, 609–629.

Deering, C. D., Bachmann, O., Dufek, J. & Gravley, D. M. (2011*a*). Rift-related transition from andesite to rhyolite volcanism in the Taupo Volcanic Zone (New Zealand) controlled by crystal–melt dynamics in mush zones with variable mineral assemblages. *Journal of Petrology* **52**, 2243–2263.

Deering, C. D., Cole, J. W. & Vogel, T. A. (2011*b*). Extraction of crystal-poor rhyolite from a hornblende-bearing intermediate mush: a case study of the caldera-forming Matahina eruption, Okataina volcanic complex. *Contributions to Mineralogy and Petrology* **161**, 129–151.

de Silva, S. L. & Gosnold, W. D. (2007). Episodic construction of batholiths: Insights from the spatiotemporal development of an ignimbrite flare-up. *Journal of Volcanology and Geothermal Research* **167**, 320–335.

Dufek, J. & Bachmann, O. (2010). Quantum magmatism: Magmatic compositional gaps generated by melt–crystal dynamics. *Geology* **38**, 687–690.

Dunbar, N. W. & Kyle, P. R. (1989). Evidence for limited zonation in silicic magma systems, Taupo Volcanic Zone, New Zealand. *Geology* **17**, 234–236.

Ellis, B. S. & Wolff, J. A. (2012). Complex storage of rhyolite in the central Snake River Plain. *Journal of Volcanology and Geothermal Research* **211–212**, 1–11.

Ewart, A. (1966). Review of mineralogy and chemistry of the acidic volcanic rocks of Taupo Volcanic Zone, New Zealand. *Bulletin of Volcanology* **29**, 147–171.

Ewart, A., Hildreth, W. & Carmichael, I. S. E. (1975). Quaternary acid magma in New Zealand. *Contributions to Mineralogy and Petrology* **51**, 1–27.

Folch, A. & Martí, J. (1998). The generation of overpressure in felsic magma chambers by replenishment. *Earth and Planetary Science Letters* **163**, 301–314.

Fridrich, C. J. & Mahood, G. A. (1987). Compositional layers in the zoned magma chamber of the Grizzly Peak Tuff. *Geology* **15**, 299–303.

Gelman, S. E., Gutierrez, F. J. & Bachmann, O. (2013). On the longevity of large upper crustal silicic magma reservoirs. *Geology* **41**, 759–762, doi:10.1130/G34241.1.

Geyer, A. & Martí, J. (2008). The new worldwide collapse caldera database (CCDB): A tool for studying and understanding caldera processes. *Journal of Volcanology and Geothermal Research* **175**, 334–354.

Ghiorso, M. S. & Evans, B. W. (2008). Thermodynamics of rhombohedral oxide solid solutions and a revision of the Fe–Ti two-oxide geothermometer and oxygen-barometer. *American Journal of Science* **308**, 957–1039.

Gravley, D. M. (2004). The Ohakuri pyroclastic deposits and the evolution of the Rotorua–Ohakuri volcanotectonic depression. PhD thesis, University of Canterbury, Christchurch, 245 p.

Gravley, D. M., Wilson, C. J. N., Leonard, G. S. & Cole, J. W. (2007). Double trouble: Paired ignimbrite eruptions and collateral subsidence in the Taupo Volcanic Zone, New Zealand. *Geological Society of America Bulletin* **119**, 18–30.

Gravley, D. M., Leonard, G. S., Wilson, C. J. N., Rowland, J. V. & Hikuroa, D. C. H. (2009). Build-up to an ignimbrite flare-up: Geologic evidence for magmatic–tectonic–volcanic interplay in the Central Taupo Volcanic Zone, New Zealand. *Geological Society of America, Abstracts with Programs* **41**, 57.

Gualda, G. A. R. & Ghiorso, M. S. (2013*a*). Low pressure origin of high-silica rhyolites and granites. *Journal of Geology* **121**, 537–545.

Gualda, G. A. R. & Ghiorso, M. S. (2013*b*). The Bishop Tuff giant magma body: An alternative to the standard model. *Contributions to Mineralogy and Petrology* **166**, 755–775.

Gualda, G. A. R. & Ghiorso, M. S. (2014). Phase-equilibrium geobarometers for silicic rocks based on rhyolite-MELTS. Part 1: Principles, procedures, and evaluation of the method. *Contributions to Mineralogy and Petrology* , in press.

Gualda, G. A. R., Ghiorso, M. S., Lemons, R. V. & Carley, T. L. (2012*a*). Rhyolite-MELTS: a modified calibration of MELTS optimized for silica-rich, fluid-bearing magmatic systems. *Journal of Petrology* **53**, 875–890.

Gualda, G. A. R., Pamukcu, A. S., Ghiorso, M. S., Anderson, A. T., Sutton, S. R. & Rivers, M. L. (2012*b*). Timescales of quartz crystallization and the longevity of the Bishop giant magma body. *PloS One* **7**, e37492.

Harrison, A. & White, R. S. (2006). Lithospheric structure of an active backarc basin: the Taupo Volcanic Zone, New Zealand. *Geophysical Journal International* **167**, 968–990.

Hildreth, W. (1981). Gradients in silicic magma chambers: implications for lithospheric magmatism. *Journal of Geophysical Research* **86**, 10153–10192.

Hildreth, W. (2004). Volcanological perspectives on Long Valley, Mammoth Mountain, and Mono Craters: several contiguous but discrete systems. *Journal of Volcanology and Geothermal Research* **136**, 169–198.

Hildreth, W. & Fierstein, J. (2000). Katmai volcanic cluster and the great eruption of 1912. *Geological Society of America Bulletin* **112**, 1594–1620.

Hildreth, W. & Wilson, C. J. N. (2007). Compositional zoning of the Bishop Tuff. *Journal of Petrology* **48**, 951–999.

Holtz, F., Pichavant, M., Barbey, P. & Johannes, W. (1992). Effects of H_2O on liquidus phase relations in the haplogranite system at 2 and 5 kbar. *American Mineralogist* **77**, 1223–1241.

Houghton, B. F., Wilson, C. J. N., McWilliams, M. O., Lanphere, M. A., Weaver, S. D., Briggs, R. M. & Pringle, M. S. (1995). Chronology and dynamics of a large silicic magmatic system: Central Taupo Volcanic Zone, New Zealand. *Geology* **23**, 13–16.

Huang, R. & Audétat, A. (2012). The titanium-in-quartz (TitaniQ) thermobarometer: A critical examination and re-calibration. *Geochimica et Cosmochimica Acta* **84**, 75–89.

Huber, C., Bachmann, O. & Manga, M. (2010). Two competing effects of volatiles on heat transfer in crystal-rich magmas: thermal insulation vs defrosting. *Journal of Petrology* **51**, 847–867.

Jarosewich, E., Nelen, J. A. & Norberg, J. A. (1980). Reference samples for electron microprobe analysis. *Geostandards Newsletter* **4**, 43–47.

Johnson, E. R., Kamenetsky, V. S., McPhie, J. & Wallace, P. J. (2011). Degassing of the H_2O-rich rhyolites of the Okataina Volcanic Center, Taupo Volcanic Zone, New Zealand. *Geology* **39**, 311–314.

Karhunen, R. A. (1993). The Pokai and Chimp Ignimbrites of NW Taupo Volcanic Zone. PhD thesis, University of Canterbury, Christchurch, 356 p.

Kennedy, B. M. & Stix, J. (2007). Magmatic processes associated with caldera collapse at Ossipee ring dyke, New Hampshire. *Geological Society of America Bulletin* **119**, 3–17.

Kennedy, B. M., Jellinek, M. A. & Stix, J. (2008). Coupled caldera subsidence and stirring inferred from analogue models. *Nature Geoscience* **1**, 385–389.

Lahitte, P., Gillot, P. & Courtillot, V. (2003). Silicic central volcanoes as precursors to rift propagation: The Afar case. *Earth and Planetary Science Letters* **207**, 103–116.

Landtwing, M. R. & Pettke, T. (2005). Relationships between SEM–cathodoluminescence response and trace-element composition of hydrothermal vein quartz. *American Mineralogist* **90**, 122–131.

Lara, L. E., Naranjo, J. A. & Moreno, H. (2004). Rhyodacitic fissure eruption in Southern Andes (Cordón Caulle; 40·5°S) after the 1960 (Mw: 9·5) Chilean earthquake: a structural interpretation. *Journal of Volcanology and Geothermal Research* **138**, 127–138.

Leonard, G. S., Cole, J. W., Nairn, I. A. & Self, S. (2002). Basalt triggering of the *c.* AD 1305 Kaharoa rhyolite eruption, Tarawera Volcanic Complex, New Zealand. *Journal of Volcanology and Geothermal Research* **115**, 461–486.

Lindsay, J., Schmitt, A. K., Trumbull, R. B., de Silva, S. L., Siebel, W. & Emmermann, R. (2001). Magmatic evolution of the La Pacana caldera system, Central Andes, Chile: Compositional variation of two cogenetic, large-volume felsic ignimbrites. *Journal of Petrology* **42**, 459–486.

Lipman, P.W. (1967). Mineral and chemical variations within an ash-flow sheet from Aso caldera, South Western Japan. *Contributions to Mineralogy and Petrology* **16**, 300–327.

Lipman, P.W. (2007). Incremental assembly and prolonged consolidation of Cordilleran magma chambers: Evidence from the Southern Rocky Mountain volcanic field. *Geosphere* **3**, 1–29.

Liu, Y., Anderson, A. T., Wilson, C. J. N., Davis, A. M. & Steele, I. M. (2006). Mixing and differentiation in the Oruanui rhyolitic magma, Taupo, New Zealand: evidence from volatiles and trace elements in melt inclusions. *Contributions to Mineralogy and Petrology* **151**, 71–87.

Manga, M. & Brodsky, E. (2006). Seismic triggering of eruptions in the far field: Volcanoes and Geysers. *Annual Review of Earth and Planetary Sciences* **34**, 263–291.

Matthews, N. E., Pyle, D. M., Smith, V. C., Wilson, C. J. N., Huber, C. & Hinsberg, V. (2011). Quartz zoning and the pre-eruptive evolution of the ~340-ka Whakamaru magma systems, New Zealand. *Contributions to Mineralogy and Petrology* **163**, 87–107.

Miller, C. F., Furbish, D. J., Walker, B. A., Claiborne, L. L., Koteas, G. C., Bleick, H. A. & Miller, J. S. (2011). Growth of plutons by incremental emplacement of sheets in crystal-rich host: Evidence from Miocene intrusions of the Colorado River region, Nevada, USA. *Tectonophysics* **500**, 65–77.

Milner, D. M. (2001). The structure and eruptive history of Rotorua caldera, Taupo Volcanic Zone, New Zealand. PhD thesis, University of Canterbury, Christchurch, 434 p.

Milner, D. M., Cole, J. W. & Wood, C. P. (2002). Asymmetric, multiple-block collapse at Rotorua Caldera, Taupo Volcanic Zone, New Zealand. *Bulletin of Volcanology* **64**, 134–149.

Milner, D., Cole, J. & Wood, C. (2003). Mamaku Ignimbrite: a caldera-forming ignimbrite erupted from a compositionally zoned magma chamber in Taupo Volcanic Zone, New Zealand. *Journal of Volcanology and Geothermal Research* **122**, 243–264.

Morgan, G. B. & London, D. (1996). Optimizing the electron microprobe analysis of hydrous alkali aluminosilicate glasses. *American Mineralogist* **81**, 1176–1185.

Naruo, H. & Kobayashi, T. (2002). Two large-scale earthquakes triggered by a 6·5 ka BP eruption from Kikai caldera, southern Kyushu, Japan. *Quaternary Research, Japan* **41**, 287–299.

Pallister, J., Hoblitt, R. & Reyes, A. (1992). A basalt trigger for the 1991 eruptions of Pinatubo volcano? *Nature* **356**, 426–428.

Peppard, B. T., Steele, I. M., Davis, A. M., Wallace, P. J. & Anderson, A. T. (2001). Zoned quartz phenocrysts from the rhyolitic Bishop Tuff. *American Mineralogist* **86**, 1034–1052.

Reubi, O. & Nicholls, I. A. (2005). Structure and dynamics of a silicic magmatic system associated with caldera-forming eruptions at Batur Volcanic Field, Bali, Indonesia. *Journal of Petrology* **46**, 1367–1391.

Roedder, E. (ed.) (1984). *Fluid Inclusions. Mineralogical Society of America, Reviews in Mineralogy* **12**, 644 p.

Rogan, M. (1982). A geophysical study of the Taupo Volcanic Zon New Zealand. *Journal of Geophysical Research* **87**, 4073–4088.

Rooney, T. O. & Deering, C. D. (2014). Conditions of melt generation beneath the Taupo Volcanic Zone: The influence of heterogeneous mantle inputs on large-volume silicic systems. *Geology* **42**, 3–6.

Rowland, J. V., Wilson, C. J. N. & Gravley, D. M. (2010). Spatial and temporal variations in magma-assisted rifting, Taupo Volcanic Zone, New Zealand. *Journal of Volcanology and Geothermal Research* **190**, 89–108.

Schmitz, M. D. & Smith, I. E. M. (2004). The petrology of the Rotoiti eruption sequence, Taupo Volcanic Zone: an example of fractionation and mixing in a rhyolitic system. *Journal of Petrology* **45**, 2045–2066.

Seebeck, H., Nicol, A., Stern, T. A., Bibby, H. M. & Stagpoole, V. (2010). Fault controls on the geometry and location of the Okataina Caldera, Taupo Volcanic Zone, New Zealand. *Journal of Volcanology and Geothermal Research* **190**, 136–151.

Shane, P., Martin, S. B., Smith, V. C., Beggs, K. F., Darragh, M. B., Cole, J. W. & Nairn, I. A. (2007). Multiple rhyolite magmas and basalt injection in the 17·7 ka Rerewhakaaitu eruption episode from Tarawera volcanic complex, New Zealand. *Journal of Volcanology and Geothermal Research* **164**, 1–26.

Shane, P., Nairn, I. A., Smith, V. C., Darragh, M., Beggs, K. & Cole, J. W. (2008). Silicic recharge of multiple rhyolite magmas by basaltic intrusion during the 22.6 ka Okareka Eruption Episode, New Zealand. *Lithos* **29**, 527–549.

Shane, P., Storm, S., Schmitt, A. & Lindsay, J. (2012). Timing and conditions of formation of granitoid clasts erupted in recent pyroclastic deposits from Tarawera Volcano (New Zealand). *Lithos* **140–141**, 1–10.

Smith, R. L. & Bailey, R. A. (1966). The Bandelier Tuff: a study of ash-flow eruption cycles from zoned magma chambers. *Bulletin of Volcanology* **29**, 83–103.

Smith, V., Shane, P. & Nairn, I. (2010). Insights into silicic melt generation using plagioclase, quartz and melt inclusions from the caldera-forming Rotoiti eruption, Taupo volcanic zone, New Zealand. *Contributions to Mineralogy and Petrology* **160**, 951–971.

Sparks, S. R. J., Sigurdsson, H. & Wilson, L. (1977). Magma mixing: a mechanism for triggering acid explosive eruptions. *Nature* **267**, 315–318.

Storm, S., Shane, P., Schmitt, A. K. & Lindsay, J. M. (2011). Contrasting punctuated zircon growth in two syn-erupted rhyolite magmas from Tarawera volcano: Insights to crystal diversity in magmatic systems. *Earth and Planetary Science Letters* **301**, 511–520.

Thomas, J. B., Watson, E. B., Spear, F. S., Shemella, F. S., Nayak, S. K. & Lanzirotti, A. (2010). TitaniQ under pressure: the effect of pressure and temperature on the solubility of Ti in quartz. *Contributions to Mineralogy and Petrology* **160**, 743–759.

Tuttle, O. F. & Bowen, N. L. (1958). *Origin of Granite, in the Light of Experimental Studies in the System $NaAlSi_3O_8$–$KAlSi_3O_8$–SiO_2–H_2O. Geological Society of America, Memoirs* **74**, 153 p.

Wallace, L. M., McCaffrey, R. & Desmond, D. (2004). Subduction zone coupling and tectonic block rotations in the North Island, New Zealand. *Journal of Geophysical Research* **109**, 1–21.

Walter, T. R. & Amelung, F. (2007). Volcanic eruptions following M ≥ 9 megathrust earthquakes: Implications for the Sumatra–Andaman volcanoes. *Geology* **35**, 539–542.

Wark, D. A. & Spear, F. S. (2005). Ti in quartz: Cathodoluminescence and thermometry. *Geochimica et Cosmochimica Acta* **69**, Supplement, A592.

Wark, D. A. & Watson, E. B. (2006). TitaniQ: a titanium-in-quartz geothermometer. *Contributions to Mineralogy and Petrology* **152**, 743–754.

Wark, D. A., Hildreth, W., Spear, F. S., Cherniak, D. J. & Watson, E. B. (2007). Pre-eruption recharge of the Bishop magma system. *Geology* **35**, 235–238.

Wiebe, R. A., Wark, D. A. & Hawkins, D. P. (2007). Insights from quartz cathodoluminescence zoning into crystallization of the Vinalhaven granite, coastal Maine. *Contributions to Mineralogy and Petrology* **154**, 439–453.

Wilcock, J., Goff, F., Minarik, W. G. & Stix, J. (2012). Magmatic recharge during the formation and resurgence of the Valles Caldera, New Mexico, USA: evidence from quartz compositional zoning and geothermometry. *Journal of Petrology* **54**, 635–664.

Wilson, C. J. N. & Charlier, B. L. A. (2009). Rapid rates of magma generation at contemporaneous magma systems, Taupo Volcano, New Zealand: insights from U–Th model-age spectra in zircons. *Journal of Petrology* **50**, 875–907.

Wilson, C. J. N., Rogan, A. M., Smith, I. E. M., Northey, D. J., Nairn, I. A. & Houghton, B. F. (1984). Caldera volcanoes of the Taupo Volcanic Zone, New Zealand. *Journal of Geophysical Research* **89**, 8463–8484.

Wilson, C. J. N., Houghton, B. F., Mcwilliams, M. O., Lanphere, M. A., Weaver, S. D. & Briggs, R. M. (1995). Volcanic and structural evolution of Taupo Volcanic Zone, New Zealand: a review. *Journal of Volcanology and Geothermal Research* **68**, 1–28.

Wilson, C. J. N., Blake, S., Charlier, B. L. A. & Sutton, A. (2006). The 26·5 ka Oruanui eruption, Taupo Volcano, New Zealand: development, characteristics and evacuation of a large rhyolitic magma body. *Journal of Petrology* **47**, 35–69.

Wilson, C. J. N., Gravley, D. M., Leonard, G. S. & Rowland, J. V. (2009). Volcanism in the central Taupo Volcanic Zone, New Zealand: tempo styles and controls. In: Thordarson, T., Larsen, G., Rowland, S. K., Self, S. & Hoskuldsson, (eds) *Studies in Volcanology: The Legacy of George Walker. Special Publications of IAVCEI* **2**, 225–247.